polysaccharides

MDPI

Article

Sequential Electrospinning of Asymmetric PDLLA/PVP-HA Scaffolds Functionalized with Glycine for Medical Devices

Antonio Laezza [1,†], Francesca Armiento [1,†], Luigi Fabiano [2], Serena Munaò [3], Paola Campione [2], Matteo Carrozzino [1], Ileana Ielo [3], Katja Schenke-Layland [4,5], Giovanna De Luca [3], Grazia Maria Lucia Messina [2], Giovanna Calabrese [3], Antonietta Pepe [1,*] and Brigida Bochicchio [1,*]

[1] Department of Basic and Applied Sciences (DISBA), University of Basilicata, Via Ateneo Lucano 10, 85100 Potenza, Italy; antonio.laezza@unibas.it (A.L.); francesca.armiento@unibas.it (F.A.); matteo.carrozzino@studenti.unibas.it (M.C.)
[2] Department of Chemical Sciences, University of Catania and CSGI, Viale A. Doria 6, 95125 Catania, Italy; luigi.fabiano@phd.unict.it (L.F.); paola.campione@unict.it (P.C.); gml.messina@unict.it (G.M.L.M.)
[3] Department of Chemical, Biological, Pharmaceutical and Environmental Sciences (ChiBioFarAm), University of Messina, Viale F. Stagno d'Alcontres 31, 98166 Messina, Italy; serena.munao@studenti.unime.it (S.M.); ileana.ielo1@unime.it (I.I.); giovanna.deluca@unime.it (G.D.L.); gcalabrese@unime.it (G.C.)
[4] NMI Natural and Medical Sciences Institute at the University of Tübingen, 72770 Reutlingen, Germany
[5] Department of Women's Health, Research Institute for Women's Health, Eberhard-Karls-University Tübingen, 72076 Tübingen, Germany
* Correspondence: antonietta.pepe@unibas.it (A.P.); brigida.bochicchio@unibas.it (B.B.)
† These authors contributed equally to this work.

Abstract

In this study we engineered bilayered electrospun scaffolds consisting of a hydrophobic PDLLA and hydrophilic PVP layer that incorporate either native HA or semi-synthetic HA-Gly-OH at concentrations of 1% and 3% *w*/*w*. Generally, bilayer scaffolds electrospun on different days delaminated, while herein they maintained their integrity because they were electrospun on the same day. Sequential electrospinning enabled the bilayer structure characterized via Scanning Electron Microscopy (SEM), Atomic Force Microscopy (AFM), and Young's modulus measurements to assess morphology and mechanics. In vitro cytotoxicity and cell viability assays with fibroblast cells confirmed good biocompatibility for both the individual layers and the bilayer system. Among the tested formulations, the bilayer PDLLA/PVP–HA-Gly-OH 1% showed the most promising performance, attributed to the synergistic effects of HA and Gly-OH in promoting adhesion and proliferation.

Keywords: bilayer scaffolds; hyaluronic acid; glycine; electrospun scaffolds; biocompatibility

Academic Editor: Ioannis S. Chronakis

Received: 5 December 2025
Revised: 6 March 2026
Accepted: 8 April 2026
Published: 13 April 2026

1. Introduction

Skin is a complex three-layered organ representing the body's primary barrier against external risks, including pathogenic microorganisms, physical trauma, and chemical stressors [1–4]. It plays a critical role in immune surveillance and maintaining homeostasis, acting as the body's frontline defense and preserving overall health. When this barrier is compromised due to injury, the body initiates a dynamic and highly regulated wound healing process, which involves overlapping stages of hemostasis, inflam-

mation, proliferation, and maturation [5]. The final phase of remodeling results in the formation of scar tissue mainly composed of collagen fibers [6].

Traditional wound dressings are primarily designed to protect clean and dry wounds from external contamination. However, they lack the ability to actively promote tissue regeneration or accelerate the healing process. To overcome these limitations, recent research has been focused on advanced wound care strategies that incorporate bioactive components and functional materials. Among these innovations, biomaterial scaffolds have emerged as a particularly promising approach [7,8]. These scaffolds function as temporary templates that facilitate cell infiltration, proliferation, and tissue regeneration by mimicking the native extracellular matrix (ECM) and providing a supportive microenvironment favorable to new tissue formation. Within this context, various fabrication methods and compositions have been investigated [9]. Particularly, electrospinning has gained attention for its ability to produce well-organized nanofibrous structures with high surface/volume ratios and interconnected porosity. These structural features are essential for maintaining a moist wound environment, allowing gas exchange, and controlling bleeding, important factors that contribute to effective wound healing [10–12].

To mimic the structural and functional features of the epidermal and dermal layers of the skin, a bilayer system has emerged as a promising strategy for enhancing wound healing [13,14]. These systems are typically engineered with an asymmetric architecture that mimics the skin's natural barrier and regenerative properties. The external layer, designed to simulate the epidermis, is typically fabricated by hydrophobic nanofibers, acting as a protective shield against external agents, such as pathogens and environmental stressors [15]. Otherwise, the inner layer consists of hydrophilic nanofibers closely resembling the ECM, thereby supporting cellular activities essential for tissue regeneration [16]. Among the methods for developing asymmetric scaffolds, sequential electrospinning is widely used [17]. It refers to one-by-one electrospinning of different material solutions or melts. In our case, it consists in fabricating hydrophobic and hydrophilic layers through one spinneret per step, leading to a bilayer architecture that provides a moist wound environment that facilitates cellular adhesion, migration, and proliferation, which are key processes in effective wound healing.

As a principal component of the ECM, hyaluronic acid (HA), also known as hyaluronan, has gained great attention for the development of innovative wound dressings [18]. HA is a non-sulfated component of glycosaminoglycans (GAGs), which is composed of D-glucuronic acid (GlcA) and *N*-acetyl-D-glucosamine (GlcNAc), linked by alternating β-1 → 3 and β-1 → 4 glycosidic bonds, resulting in 4)-β-GlcA-(1 → 3)-β-GlcNAc-(1 → disaccharide repeating unit. HA plays important roles in the healing process, participating in inflammation modulation, angiogenesis, and tissue remodeling [19,20]. In addition to its biocompatibility and biodegradability, the presence of functional groups along its polysaccharide backbone, specifically hydroxyl and carboxyl groups, confers high hydrophilicity that facilitates exudate absorption [21]. Moreover, these functional groups also enable the functionalization of the backbone for obtaining tailored derivatives [18,22].

Pure and functionalized HA have been investigated for nanofibrous wound dressing production. However, the high viscosity of their solutions limits the polysaccharide spinnability, a drawback that has been addressed by blending HA with different natural and synthetic polymers [23–25]. Among them, polyvinylpyrrolidone (PVP) presents water solubility, chemical inertness, thermal stability, pH resistance, non-toxic nature, and non-ionic character. These features have made PVP a valuable component in electrospun materials for wound dressings and a wide range of other biomedical applications [26,27].

This work aims to fabricate, by sequential electrospinning, an asymmetric or bilayer scaffold containing poly-D,L-lactide (PDLLA) and a PVP/HA-Gly-OH blend serving as hydrophobic and hydrophilic layers, respectively. Without a doubt, for many years, L-alpha amino acid residues of certain biological relevance have been grafted with HA in aqueous solution via amide bond formation through carbodiimide/*N*-hydroxysuccinimide chemistry in order to synthesize HA derivatives empowered in terms of biocompatibility with added value in tissue engineering and regenerative medicine [28,29]. At the same time, electrospinning is a precious technique aimed at the production of microfibers hierarchically organized in interconnected porous structures, assuring nutrients and waste exchanges essential for the survival of cells. On that basis, HA has been widely electrospun with synthetic or natural polymers for the production of hybrid scaffolds with several applications in biomedicine.

Although the literature widely reports the use of native HA in the fabrication of electrospun asymmetric scaffolds [24,30–32], the application of suitably functionalized glycosaminoglycan in the design of these materials has not yet been fully explored. The novelty of this work consists in the electrospinning of covalently functionalized HA [23].

A strategic localization of semi-synthetic HA-Gly-OH exclusively within the hydrophilic layer could create a spatially defined bioactive interface for cells, while the external PDLLA layer remains an unmodified mechanical barrier. While polysaccharide-glycine peptide conjugates have been incorporated into biomaterials [33–36], this study aims to address the gap in current knowledge by examining the functionalization of HA with the single amino acid glycine. Our approach involves the functionalization of HA with this small molecule to investigate its impact on the scaffolds' physico-chemical properties while introducing beneficial chemical motifs, without the added complexity and cost associated with peptide synthesis.

The developed scaffold will be thoroughly characterized in terms of its morphological properties using scanning electron microscopy (SEM). Additionally, its biocompatibility will be assessed through in vitro assays, including cell viability (MTT or Live/Dead staining), cell adhesion, and proliferation studies using fibroblast cell lines to evaluate its potential for clinical wound healing applications.

2. Materials and Methods

2.1. Materials

Commercial-grade reagents and solvents were used without further purification, except where otherwise indicated. The term "ultrapure water (UPW)" refers to water purified by a Millipore Milli-Q Gradient system. (Young Lin, Korea) HA (Mw = 186 KDa) medical device grade was a generous gift of Altergon Italia SrL (Morra de Sanctis, AV, Italy). Hydrochloric acid 37% (HCl) and sulfphuric acid 95% (H_2SO_4) were purchased from VWR (Milan, Italy). 2-(*N*-Morpholino)ethanesulfonic acid hydrate (MES), 3-(Trimethylsilyl)propionic-2,2,3,3-d_4 acid sodium salt (DSS), glycine ethyl ester hydrochloride (Gly-OEt·HCl), cetyltrimetyl ammonium bromide (CTAB), glacial acetic acid (AcOH), phenol, PVP (Mw ~1300 KDa), sodium acetate trihydrate ($AcONa{\cdot}3H_2O$), sodium chloride (NaCl), and sodium hydroxide pellets (NaOH) were purchased from Sigma Aldrich (Milan, Italy). 1,1,1,3,3,3-Hexafluoro-2-propanol (HFP) and *N*-(3-(Dimethylamino)propyl)-*N*′-ethylcarbodiimide hydrochloride (EDC·HCl) was purchased from Iris Biotech GmbH (Marktredwitz, Germany), and *N*-Hydroxysulfosuccinimide sodium salt (s-NHS) was purchased from TCI Chemicals (Tokyo, Japan). PDLLA (EasyFil PLA, transparent pellets, molecular weight: 126 KDa, density: 1240 kg/m^3) was obtained from FormFutura (Nijmegen, The Netherlands).

2.2. Methods

2.2.1. Nuclear Magnetic Resonance (NMR) Spectroscopy

NMR spectra were recorded on 500 MHz (^{1}H: 500 MHz, ^{13}C:125 MHz) and 400 MHz (^{1}H: 400 MHz, ^{13}C: 100 MHz) Inova instruments Varian (Palo Alto, CA, USA) in D_2O or 9:1 *v*/*v* H_2O/D_2O (DSS 0.1 mM as internal standard, δ_H = 0 ppm). The degree of substitution (DS) of HA-Gly-OEt is attributed to disaccharide repeating units.

2.2.2. Attenuated Total Reflectance Fourier Transform Infrared (ATR-FT-IR) Spectroscopy

ATR-FT-IR spectra were carried out on J-460 (Jasco Europe Srl, Cremella, LC, Italy) equipped with ATR an ATR PRO ONE. Single-reflection ATR accessory using a single-crystal diamond ATR prism. Spectra were acquired in the region from 4000 to 450 cm^{-1} with a spectral resolution of 2 cm^{-1} and 256 scans. Background spectra were recorded each time and then subtracted from the sample spectra.

2.2.3. Scanning Electron Microscopy (SEM)

SEM images were acquired with a voltage of 20 kV and different magnifications after gold sputter-coating on an FEI Quanta 400 high-resolution field emission scanning electron microscope (ESEM) instrument (Hillsboro, Oregon, USA). The diameter of the fibers and the porosity were evaluated using ImageJ software (version 1.49v) supplied with the DiameterJ plug-in. The sample size considered corresponds to 50 individual fibers measured from three different images obtained from one scaffold, for a total of 150. For the cross-section analysis, the samples were secured on plotted stubs and cut using fine scissors. The images were acquired with a 20 kV and different magnifications after gold sputter-coating on a Philips-FEI ESEM XL30-LaB6 instrument.

2.2.4. Atomic Force Microscopy (AFM)

The mechanical properties of the electrospun fibers were evaluated by force spectroscopy using an NTEGRA II AFM (NT-MDT, Moscow, Russia). Force–distance curves were collected, and the Young's modulus was extracted from the elastic portion of the curves. Stiff single-crystal silicon cantilevers with a symmetric tip geometry were employed (model Tap300AI-G, BudgetSensors, Sofia, Bulgaria; nominal resonance frequency 300 kHz, nominal spring constant 40 N m^{-1}, and tip radius < 10 nm). The spring constant of each cantilever was calibrated using the Sader method [37].

The Young's modulus was obtained by fitting the experimental force–distance curves in the elastic regime with the Derjaguin–Muller–Toporov (DMT) model [38], according to the Equation (1):

$$F + F_{ad} = \frac{4E_s}{3(1-\nu_s^2)}\sqrt{R\delta^3} \quad (1)$$

where F is the applied force; F_{ad} is the adhesion force; E_s is Young's modulus; ν_s is Poisson's ratio for the sample; R is the radius of the spherical indenter; and δ is the elastic indentation depth. A Poisson's ratio of 0.40 was chosen based on values commonly reported for amorphous polymers such as PVP under standard conditions [39,40]. It was used for all samples to enable consistent comparison among formulations; possible small variations in ν due to HA or HA–Gly–OH incorporation are not expected to affect the relative trends discussed in this work. Measurements were carried out at ambient temperature and a relative humidity of 44.72%. More than 300 force–distance curves were acquired, on each sample, in three independent measurements by collecting the curves along the fiber length, thereby ensuring that the probe indented the uppermost regions of the fibers and reducing artifacts arising from abrupt height variations of the fibrous matrix. The elastic modulus was determined from the distribution of the collected data

and analyzed using Origin 2018 software. Statistical evaluation of the datasets was subsequently performed by one-way ANOVA followed by Welch's *t*-tests in order to assess global and pairwise differences among the different formulations.

2.2.5. Semi-Synthesis of Derivative HA-Gly-OEt

HA (101.19 mg, 0.25 mmol) was suspended in pure H_2O (15.0 mL) and stirred at room temperature up to complete dissolution, then treated with a 208.30 mM EDC·HCl (2.41 mL, 0.50 mmol) and 103.29 mM s-NHS (2.43 mL, 0.25 mmol) solution. After 40 min, MES·xH_2O (44.25 mg) and 250 mM Gly-OEt·HCl (2 mL, 0.50 mmol) were added to the reaction mixture, obtaining a clear solution. Few drops of freshly prepared 1.0 M NaOH solution were then added to adjust pH to 6, and stirring was continued overnight. After ~ 20 h, the crude was neutralized by HCl 1.0 M and dialyzed against NaCl 150 mM solution for 2 days and against H_2O for a further 2 days. The subsequent freeze-drying yielded a white solid (81.74 mg, yield = 77%). ^{1}H-NMR (500 MHz, D_2O): δ_{DSS} = 4.55 (H-1 GlcNAc), 4.46 (H-1 GlcA), 4.24 (CH_2 Gly-OEt), 4.00–3.20 (H-2, H-3, H-4, H-5 GlcA, H-2, H-3, H-4, H-5, H-6 GlcNAc), 2.01 (CH_3 GlcNAc), 1.27 (CH_3 Gly-OEt).

2.2.6. Semi-Synthesis of Derivative HA-Gly-OH

HA-Gly-OEt (81.04 mg, 0.19 mmol) was treated with a 1.0 M NaOH (10 mL) solution to adjust pH to 12. The solution was stirred for 6 h at rt, and then 1 M HCl was added until neutralization. Dialysis and subsequent freeze-drying yielded a white solid (59.68 mg, yield = 70%). ^{1}H-NMR (500 MHz, D_2O): δ_{DSS} = 4.55 (H-1 GlcNAc), 4.46 (H-1 GlcA), 4.00–3.20 (H-2, H-3, H-4, H-5 GlcA, H-2, H-3, H-4, H-5, H-6 GlcNAc), and 2.01 (CH_3 GlcNAc).

2.2.7. Electrospinning

Electrospinning was performed on a Linari EngineeringGamma-High-Voltage generator electrospinning system (Pisa, Italy), and the composition of the electrospinning solutions is reported in Table 1.

Table 1. Composition of the electrospinning solution.

Hydrophobic Layer						
Scaffold	**PDLLA (% *w*/*V*)**		**HFP (mL)**			**Final Volume (mL)**
PDLLA	12.0		2.0			2.0
Hydrophilic Layer						
Scaffold	**PVP (% *w*/*V*)**	**HA (% *w*/*w*)**	**HA-Gly-OH (% *w*/*w*)**	**H_2O (mL)**	**EtOH (mL)**	**Final Volume (mL)**
PVP	10.0	-	-	0.4	1.6	2.0
PVP-HA 1%	10.0	1.0	-	0.4	1.6	2.0
PVP-HA 3%	10.0	3.0	-	0.4	1.6	2.0
PVP-HA-Gly-OH 1%	10.0	-	1.0	0.4	1.6	2.0
PVP-HA-Gly-OH 3%	10.0		3.0	0.4	1.6	2.0

In the case of the hydrophobic layer, PDLLA (240 mg) was dissolved in HFP (2.0 mL) and kept under magnetic stirring overnight at T = 37 °C. The solution was loaded into a 10 mL glass syringe with a 20 G stainless-steel needle (N) and then electrospun at an applied voltage (V) of 17 kV with a flow rate (F) of 1.0 mL/h of the pump. The target was a round copper plate having a 90 mm diameter coated with aluminum foil, and the distance (d) between the collector and the needle was set to 19 cm.

For the hydrophilic layer, the preparation of the electrospinning solutions was performed by the following general protocol: HA (2.0 mg) or HA-Gly-OH (2.0 mg), when present, was dissolved in H_2O (0.4 mL) and then left to stand for 2 h at room temperature with stirring. In parallel, PVP (200 mg) was dissolved in EtOH (0.6 mL) and also stirred for 2 h at room temperature. Subsequently, the HA or HA-Gly-OH was combined with PVP and diluted with additional EtOH (1.0 mL). The resulting mixture was stirred overnight at the temperature of 37 °C. The solution was loaded into a 10 mL glass syringe with a 20 G stainless-steel needle and then electrospun at 19 kV with a flow rate of 0.5 mL/h from the pump. The target was a round copper plate having a 90 mm diameter coated with aluminum foil, and the distance between the collector and the needle was set to 19 cm. To avoid the complete dissolution in ultrapure water of the neat PVP layer as well as of those composed of PVP and HA or PVP and HA-Gly-OH, the resulting scaffolds were crosslinked by ultraviolet radiation (254 nm) in a multiray reactor (Helios Italquartz, Milan, Italy) for 60 min, corresponding to a UV dose of 169.2 mJ/cm^2. To evaluate scaffold biocompatibility, the samples were electrospun directly onto 13 mm glass coverslips. The electrospun volume was reduced to 1.0 mL for both layers, maintaining the concentration reported above and the electrospinning conditions. Considering the reduced volume, the resulting scaffolds were irradiated for 15 min, corresponding to a UV dose of 42.3 mJ/cm^2.

2.3. Wettability (Water Contact Angle Measurement)

Surface wettability of the electrospun scaffolds was evaluated by static water contact angle (SWCA) measurements by using a Drop Shape Analyzer (DSA25E, KRÜSS) operated in sessile drop mode. A droplet of ultrapure water (2 μL) was deposited onto the scaffold surface using an automated syringe system. All measurements were performed at 20 °C. Results were calculated from nine measurements obtained from three different scaffold pieces for each sample.

The contact angle was recorded 10 s after droplet deposition to standardize the measurement and minimize the influence of rapid absorption phenomena occurring on highly hydrophilic fibrous surfaces.

2.4. Cell Culture and Biocompatibility Evaluation

To evaluate scaffold biocompatibility, L929 murine fibroblasts were used. The cells were acquired from the American Type Culture Collection (ATCC, Rockville, MD, USA) and cultured in Dulbecco's Modified Eagle Medium High Glucose (DMEM, Merck Life Science S.r.l., Milan, Italy) supplemented with 10% fetal bovine serum (FBS, Merck Life Science S.r.l., Milan, Italy) 1% penicillin/streptomycin/amphotericin B (PSA, Merck Life Science S.r.l., Milan, Italy). Cultures were maintained at 37 °C in a humidified atmosphere containing 5% CO_2 and subcultured upon reaching 80–90% confluence. Electrospun scaffolds deposited onto 13 mm glass coverslips were sterilized by UV irradiation for 30 min prior to use. L929 fibroblasts were seeded onto each scaffold at a density of 3 × 10^4 cells per sample using a dropwise technique to ensure uniform initial adhesion. The seeded scaffolds were incubated for two hours under standard culture conditions (37 °C, 5% CO_2, humidified atmosphere). Following this adhesion period, 500 μL of fresh complete culture medium was carefully added to each well to fully immerse the scaffolds and support subsequent cell growth.

Cell viability was assessed using the MTT assay [3-(4,5-dimethylthiazol-2-yl)-2,5-diphenyltetrazolium bromide] test (Merck Life Science S.r.l., Milan, Italy) at 24 and 48 h post-seeding as previously reported [41,42].

For each time point, 500 μL of a 1 mg/mL MTT solution prepared in serum-free high-glucose DMEM was added to each well and incubated at 37 °C for 2 h. The result-

ing formazan crystals were solubilized in 500 µL of dimethyl sulfoxide (DMSO; Merck Life Science S.r.l., Milan, Italy). Absorbance was measured at 540 nm using a microplate reader (AMR-100, Biosigma, Verona, Italy). Viability data were normalized to cells cultured without scaffolds, which served as the internal control.

Live/Dead staining was performed on L929 fibroblasts cultured on electrospun scaffolds for 24 and 48 h to assess cell viability and distribution, providing qualitative insights into cell proliferation and scaffold cytocompatibility. After incubation, the culture medium was carefully removed, and each scaffold was rinsed three times with phosphate-buffered saline (PBS, pH 7.4; Merck Life Science S.r.l., Milan, Italy) to eliminate residual media. A 2× working solution of the LIVE/DEAD Cell Imaging Kit (Invitrogen, Cat. No. R37601; excitation/emission: 488/570 nm; Thermo Fisher Scientific, Waltham, MA, USA) was prepared according to the manufacturer's protocol and applied to the samples. The scaffolds were then incubated with the staining solution for 30 min at room temperature in the dark to ensure optimal dye uptake and minimize photobleaching. Fluorescence imaging was performed using a NEXCOPE NE 900 inverted fluorescence microscope equipped with a digital camera (TiEsseLab S.r.l., Milan, Italy). Viable cells were visualized by green fluorescence from Calcein AM, while non-viable cells were identified by red fluorescence from BOBO-3 Iodide, enabling qualitative assessment of scaffold cytocompatibility.

2.5. Sol (SF) Gel Fraction (GF) Calculation

To evaluate the SF and GF for each sample, four pieces from three different cross-linked scaffolds (a total of 12 samples) were investigated. Each sample was immersed in UPW (10 mL) and shaken at 60 rpm on an orbital shaker at room temperature for 24 h. Thereafter, the liquid was gently removed, and the samples were freeze-dried; then the SF was calculated according to the following Equations (2) and (3):

$$SF\ (\%) = \frac{W_s - W_d}{W_s} 100 \quad (2)$$

$$GF\ (\%) = 100 - SF\ (\%) \quad (3)$$

where W*s* and W*d* are the weights of starting and freeze-dried scaffolds, respectively.

2.6. Calibration Curve for CTAB Assay

To construct a calibration curve, a 0.2 M sodium acetate buffer (pH 5.5) containing NaCl 0.15 M was freshly prepared, as well as a 2.5% *w*/*v* CTAB solution in a 2% *w*/*v* NaOH aqueous solution. The latter was stirred at 37 °C up to complete dissolution.

HA (15.0 mg) was dissolved in buffer to obtain a 3 mg/mL stock hyaluronic acid solution. Serial dilutions with the buffer were performed to obtain solutions with a final volume of 3.0 mL and with concentrations between 1.7 µg/mL and 0.4 mg/mL. From each solution, 500 µL were collected and treated with 1.0 mL of CTAB solution. Samples were incubated at 37 °C for 20 min, and the absorbance was measured at 37 °C within 10 min at λ = 570 nm using an Agilent Cary 60 ultraviolet−visible (UV−Vis) spectrophotometer. Thus, a calibration curve with the following Equation (4) was constructed:

$$Absorbance = 3.54762 * concentration \quad (4)$$

2.7. CTAB Assay for Cumulative Release

PVP-HA 1% and PVP-HA-Gly-OH 1% scaffolds have been analyzed for evaluating the native and semi-synthetic derivative release profiles. Four pieces from three different scaffolds (a total of 12 samples) were investigated by immersing each sample in a 0.2 M

sodium acetate buffer (pH 5.5) containing NaCl 0.15 M (5.0 mL) and left stirring at 37 °C. At regular intervals, 500 µL of the solution were collected and treated with 1.0 mL of 2.5% *w*/*v* CTAB solution in 2% *w*/*v* NaOH aqueous solution. Samples were incubated at 37 °C for 20 min, and the absorbance was measured within 10 min at λ = 570 nm using an Agilent Cary 60 UV−Vis spectrophotometer. The PVP scaffold as a negative control was analyzed under the same conditions, and a solution of sodium acetate buffer and CTAB was used as a blank. To maintain constant total volumes of the solutions, after each sampling, 500 µL of fresh buffer was added.

The concentrations of the released HA and HA-Gly-OH were calculated from a standard calibration curve; then, the cumulative release as a function of time was calculated according to the following Equation (5):

$$Cumulative\ release\ (\%) = \left(C_t V_{tot} + \sum_{t=0}^{k=1} f_s m_k\right)\frac{100}{Q_{tot}} \quad (5)$$

where C_t, V_{tot}, f_s, m_k, and Q_{tot} are the measured concentration at time t, the total volume used for the release test, the collected solution fraction, the amount of drug released at time k, and the theoretical drug quantity in the scaffold, respectively.

2.8. Phenol Assay

Following cumulative release, PVP-HA 1% scaffolds have been analyzed, by way of example, for hyaluronic acid content evaluation employing the phenol assay. The scaffolds have been suspended in UPW (1 mL), treated with a 5% *w*/*v* phenol aqueous solution (1 mL), and with 95% H_2SO_4 (5 mL). Samples have been incubated at 30 °C for 20 min, and the absorbance was measured at λ = 490 nm using an Agilent Cary 60 UV−Vis spectrophotometer. The PVP scaffold as a negative control was analyzed under the same conditions, and a solution of UPW, aqueous phenol, and concentrated H_2SO_4 was used as a blank.

3. Results and Discussion

3.1. Semi-Synthesis of HA-Gly-OH

The amidation of HA with glycine amino acid was accomplished with Gly-OEt·HCl in MES-buffered water (pH = 6) by employing carbodiimide chemistry for the GlcA carboxylate activation (Scheme 1). After an overnight reaction at room temperature, dialysis and freeze-drying furnished the derivative HA-Gly-OEt in 77% mass yield. The subsequent hydrolysis of the ethyl ester group under alkaline aqueous conditions afforded the derivative HA-Gly-OH in 70% mass yield after dialysis and freeze-drying.

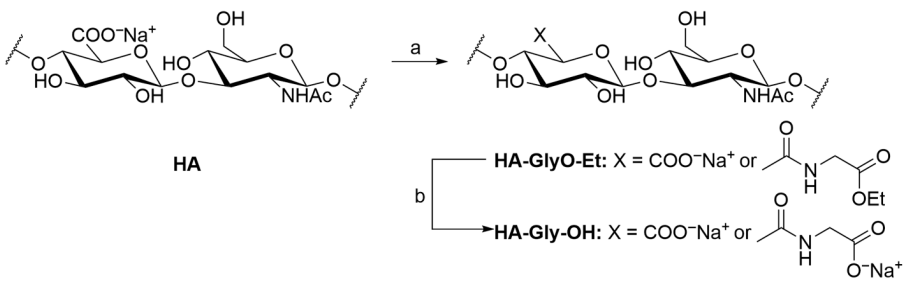

Scheme 1. Semi-synthesis of derivative HA-Gly. **a**: GlyOEt·HCl, EDC·HCl, s-NHs, MES, H_2O, pH = 6, RT, overnight, yield = 77%, DS = 0.25; **b**: NaOH, H_2O, pH = 12, RT, 6 h, yield = 70%, DS = quantitative.

^{1}H NMR analysis in D_2O confirmed the functionalization of HA thanks to the presence of signals at δ_{DSS} = 4.25 ppm and δ_{DSS} = 1.29 ppm, associated with the CH_2 and CH_3 of the amino acid ester protecting group, respectively (Figure 1, red spectrum). The DS for the HA-Gly-OEt derivative, with a value of 0.25, was calculated by comparing the integration of the Gly-OEt residue CH_3 signal with respect to those of the HA anomeric protons (δ_{DSS} = 4.64–4.38 ppm) (Figure S1) with the following Equation (6):

$$DS = \frac{\frac{2}{3} I_{CH_3(GlyOEt)}}{I_{CH\ (GlcA)+CH\ (GlcNAc)}} \quad (6)$$

The subsequent quantitative removal of ethyl ester on GlyOEt was confirmed by the absence of signals associated with the protecting group in the ^{1}H-NMR spectrum of derivative HA-Gly-OH (Figure 1, blue spectrum).

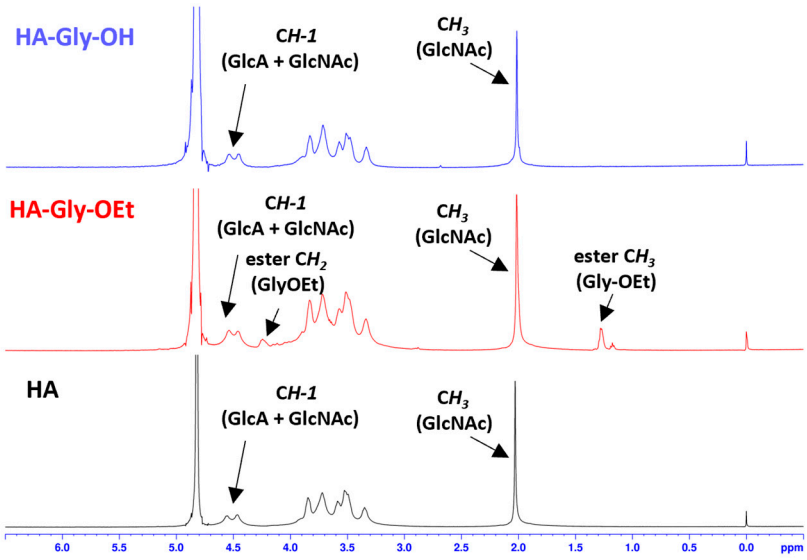

Figure 1. ^{1} H NMR spectra of HA (black), HA-Gly-OEt (red), and HA-Gly-OH (blue) (500 MHz, D_2O, 25 °C).

Furthermore, the amide region of the ^{1}H-NMR spectrum recorded in H_2O/D_2O 9:1 *v*/*v* of underivatized HA was compared with that of HA–Gly–OH to confirm the presence of the amino acid after global deprotection (Figure S2). The spectrum of native HA (black spectrum) displayed a signal at δ_{DSS} = 8.05 ppm, attributable to the amide proton of the GlcNAc residue, in agreement with literature data [43,44]. Upon functionalization with Gly–OH (Figure S2, red spectrum), an additional peak appeared at δ_{DSS} = 8.65 ppm, which can be assigned to the newly formed amide proton following HA modification (Figure S2, red spectrum). A slight downfield shift of the GlcNAc amide proton to δ_{DSS} = 8.10 ppm was also detected, suggesting a change in the local conformation of the polysaccharide backbone. Day and co-workers recently reported an opposite trend following the chemical modification of hyaluronan oligosaccharides [45].

The characterization of HA and semi-synthetic derivatives was further carried out by ATR-FT-IR (Figure 2), allowing the assignment of specific functional groups on the polysaccharide backbones. In the HA spectrum (black curve), several regions can be distinguished: the stretching vibrations of carbohydrate O-H and acetamido N-H are visible between 3500 and 3000 cm^{-1} (red circle), as well as the stretching vibrations of C-H and C-H_2 groups that are visible between 2950 and 2863 cm^{-1} (blue circle). In addition, it is visible in the 1630–1700 cm^{-1} region, corresponding to the asymmetric stretching vibrations of carboxylate and to the C=O vibrations of the acetamido group (amide I, green

circle). At ~ 1559 cm^{-1} is present the band corresponding to symmetric stretching of carboxylate and the C-N (amide II, orange circle) band of acetamido group stretching vibrations.

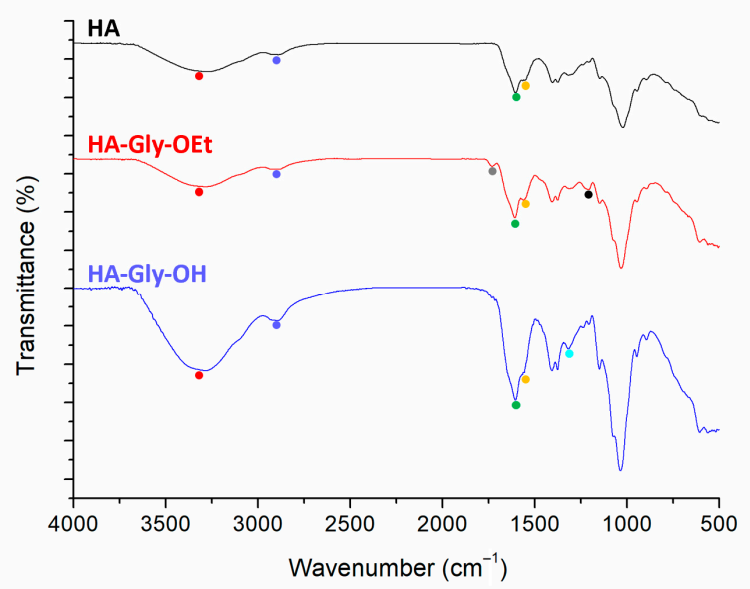

Figure 2. ATR FT-IR spectra of HA (black), HA-Gly-OEt (red), and HA-Gly-OH (blue). O-H and N-H stretching vibration band (red circle), C-H and C-H_2 stretching vibration (blue circle), ester C=O stretching vibration (grey circle), amide and carboxylate C=O stretching vibration (green circle), amide C-N and carboxylate C=O stretching vibration (orange circle), C-H_2 bending vibration (turquoise circle), ester C-O stretching vibration (black circle).

In the spectrum of HA-Gly-OEt (Figure 2, red spectrum), besides the above-mentioned bands, the occurrence of amidation is evident due to the bands at ~1730 cm^{-1} (grey circle) and ~1210 cm^{-1} (black circle), corresponding to C=O and C-O stretching vibrations of the ester protecting group of Gly-OEt [46]. Finally, the spectrum of HA-Gly-OH (Figure 2, blue spectrum) confirms the alkaline deprotection of ethyl ester, characterized by the strong band at ~1730 cm^{-1}, and at the same time the presence of the amino acid on the polysaccharide backbone thanks to the intense band at 1316 cm^{-1} associated with the bending of C-H_2 group (turquoise circle).

3.2. Electrospinning and Morphological Analysis of Electrospun Composites

Our aim is to produce asymmetric, or bilayer, electrospun scaffolds that meet the requirements of tissue engineering by the sequential electrospinning of biodegradable and bioactive polymers. Sequential electrospinning, in fact, allows the controlled deposition of different layers (Scheme 2) with distinct biological and mechanical functions [47]. As reported in Table 1, the external hydrophobic layer was prepared by dissolving neat PDLLA in HFP to a final concentration of 12.0% *w/v* solution.

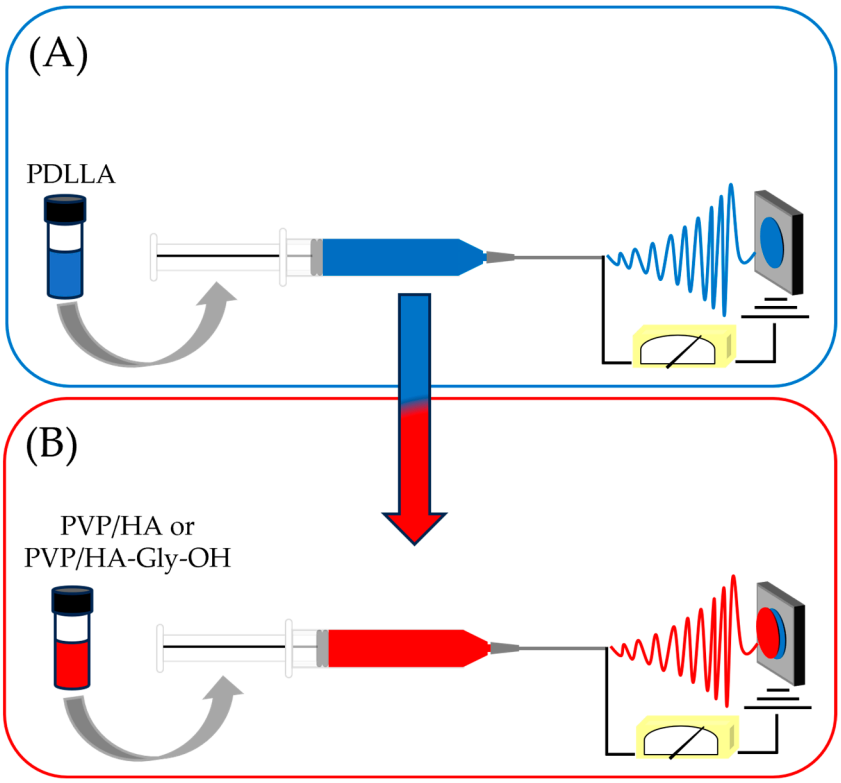

Scheme 2. Sequential electrospinning for the production of asymmetric scaffolds. (**A**): N = 20 G, V = 17 kV, F = 1.0 mL/h, d = 19 cm; (**B**) N = 18 G, V = 19 kV, F = 0.5 mL/h, d = 19 cm.

In contrast, the inner hydrophilic layers were fabricated by blending the semi-synthetic HA-Gly-OH with PVP in ethanolic aqueous solution (80% *v*/*v*). HA-Gly-OH was prepared at 1% and 3% *w*/*w* weight ratios, while PVP was at 10% *w*/*v*. Electrospinning process parameters were optimized in different conditions for the hydrophobic and hydrophilic layers to assure the process stability and afford membranes with characteristics of uniformity at the macroscopic level.

On the other hand, at the microscopy level, the final aim was to obtain defect-free scaffolds. Therefore, SEM was used to investigate the scaffolds' morphology in terms of fiber orientation, size, and diameter distribution. As a matter of facts, SEM images of all electrospun scaffolds revealed three-dimensional microstructures characterized by interconnected pores. In particular, the PDLLA scaffold (Figure 3A) displayed nearly linear, defect-free fibers with an average diameter of 1.23 ± 0.64 μm (Figure S3).

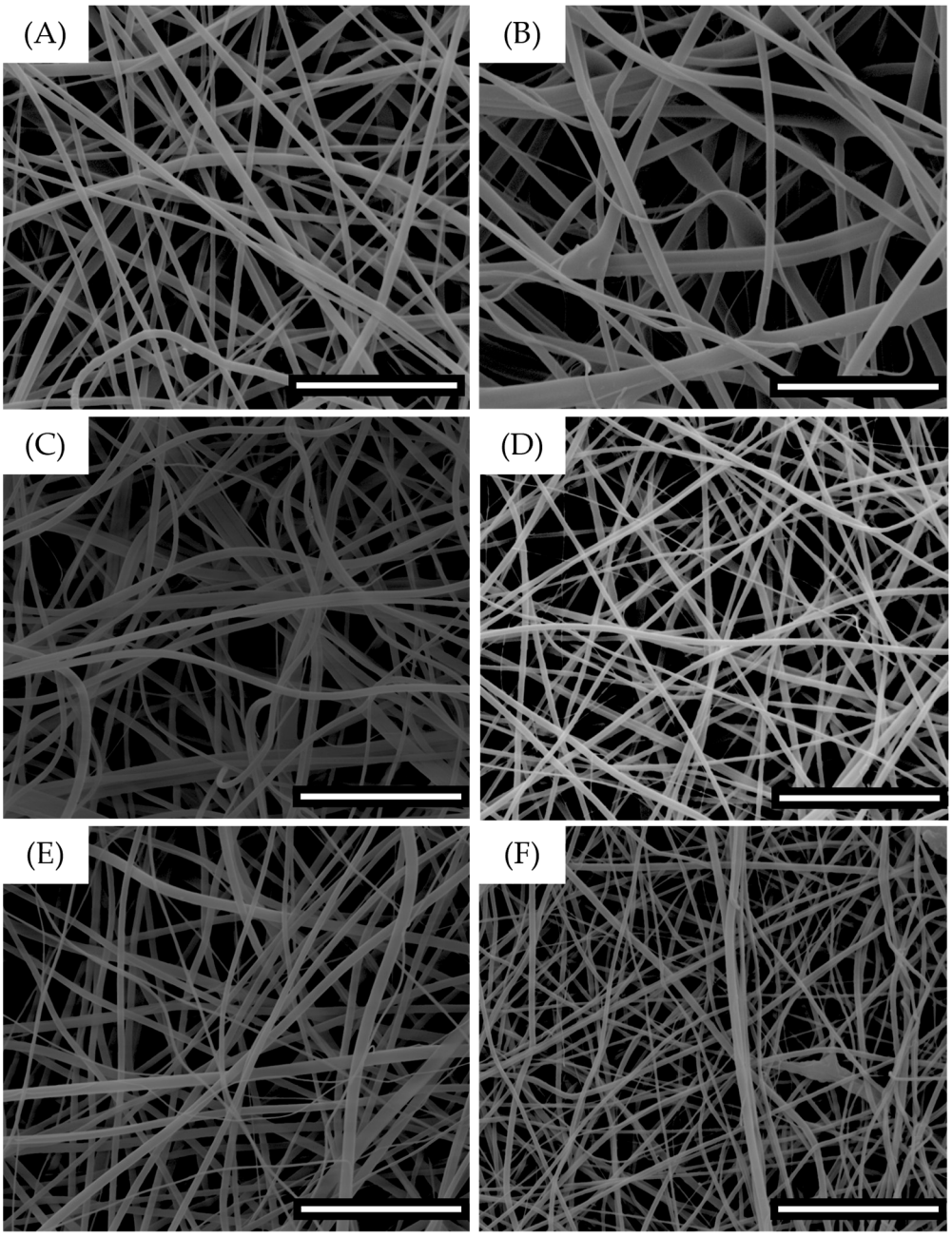

Figure 3. SEM images of electrospun scaffolds (bar: 20 μm). PDLLA (**A**), PVP (**B**), PVP-HA 1% (**C**), PVP-HA 3% (**D**), PVP-HA-Gly-OH 1% (**E**), PVP-HA-Gly-OH 3% (**F**).

Regarding the morphology of the hydrophilic layers, the scaffolds exhibited a generally homogeneous fiber distribution, which appeared slightly curled upon the addition of HA or HA-Gly-OH to PVP (Figure 3B–F). Regarding fiber size, there is an evident limitation of this study due to the lack of independent scaffold replicates, because all 150 measurements are essentially technical replicates. On that basis, fiber analysis is a qualitative study. However, the average diameters of fibers as a function of frequency (Figure S3) showed a normal distribution around mean values of 1.56 ± 0.79, 1.31 ± 0.51, and 0.95 ± 0.24 μm for PVP, PVP-HA 1%, and PVP-HA 3%, respectively, as reported in Table 2. Moreover, the incorporation of HA-Gly-OH to PVP at concentrations of 1% *w*/*w* and 3% *w*/*w* resulted in a decrease of average diameters dimensions, specifically of 1.44 ± 0.46 and 0.79 ± 0.18 μm, respectively. Interestingly, PVP-HA 3% and PVP-HA-Gly-OH 3% *w*/*w* showed the smallest average fiber diameter (0.95 ± 0.24 and 0.79 ± 0.18, respectively)

and the smallest standard deviation values as well among electrospun scaffolds (Figure 4).

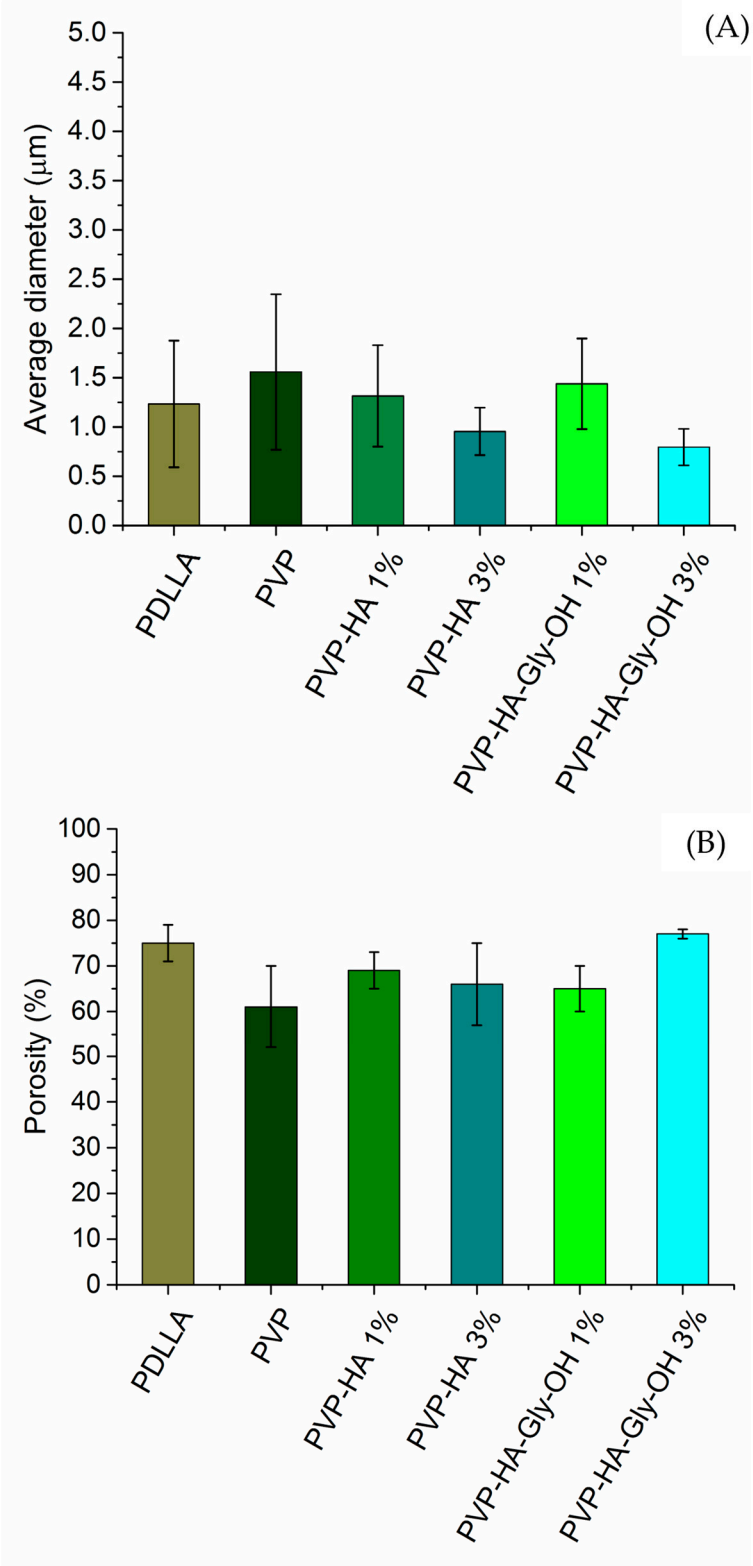

Figure 4. Mean fiber diameter (**A**) and porosity (**B**) values (±standard deviation) of electrospun scaffolds (n = 3 per group).

Table 2. Mean fiber diameter, porosity, and pore area ± standard deviation.

Scaffold	Diameter (μm)	Porosity (%)	Pore Area(μm²)
PDLLA	1.23 ± 0.64	75 ± 4	14.42 ± 3.87
PVP	1.56 ± 0.79	61 ± 9	37.6 ± 9.90
PVP-HA 1%	1.31 ± 0.51	69 ± 4	21.68 ± 4.86
PVP-HA 3%	0.95 ± 0.24	66 ± 9	7.53 ± 3.86
PVP-HA-Gly-OH 1%	1.44 ± 0.46	65 ± 5	11.31 ± 4.26
PVP-HA-Gly-OH 3%	0.79 ± 0.18	77 ± 1	30.19 ± 3.56

This behavior can be attributed to both the chemical composition and electrospinning process parameters used for the hydrophobic and hydrophilic layers. When the hydrophilic layers are compared, the PVP scaffold exhibited a higher average fiber diameter (1.56 ± 0.79 μm) than those containing HA and HA-Gly-OH. Specifically, for PVP-HA 1% and PVP-HA-Gly-OH 1%, an average fiber diameter of 1.31 ± 0.51 μm and 1.44 ± 0.46, respectively was observed. When the concentration of HA and HA-Gly-OH reached 3% *w*/*w* within the scaffold, an average fiber diameter of 0.95 ± 0.24 μm and 0.79 ± 0.18 μm was observed respectively. It is worth noting that for 1% concentration the standard deviation was twice that calculated for 3% scaffolds, thus suggesting more dispersion in the group. Taking these considerations into account, it is suggested that a general decrease of diameter values was observed upon addition of hyaluronic acid. A possible explanation for that could be found in the increased conductivity of HA-containing solutions, a phenomenon previously reported in the electrospinning of ethanolic–aqueous solutions containing HA [48]. As a proof of concept, the bioconjugation of the hydrophilic small zwitterionic amino acid Gly-OH to HA induced a further reduction of average diameter length.

The addition of HA-Gly-OH resulted in a slight variation in diameters, showing an increase at 1% *w*/*w* and a decrease at 3% *w*/*w* when compared with scaffolds containing HA at the same concentrations. Conversely, when the concentration of HA and HA-Gly-OH as well increased from 1% *w*/*w* to 3% *w*/*w*, a decrease in diameter was observed. This feature could be attributed to the higher conductivity of the electrospinning solution associated with the increased concentration of the glycosaminoglycan.

Porosity is a critical parameter that dictates cellular infiltration and tissue ingrowth into fibrous scaffolds [49]. The porosity values obtained for the scaffolds in this study are summarized in Table 2 and illustrated in Figure 4B. PDLLA scaffold displayed a porosity value of 75 ± 4%. The hydrophilic layers showed lower porosity, with values moving from 61 ± 9% for the PVP scaffold to 69 ± 4% and 66 ± 9% for PVP-HA 1% and PVP-HA 3%, respectively. In comparison, when HA-Gly-OH has been blended with PVP, the measured porosity increased from 65 ± 5% to 77 ± 1% for PVP-HA-Gly-OH 1% and PVP-HA-Gly-OH 3%, respectively.

The area of pores was also investigated, and the data distribution showed a similar trend across the five scaffolds (Figure S4). Since the values followed a log-normal distribution, the mean pore area for each scaffold was calculated using the geometric mean [50]. The mean pore areas for PDLLA and PVP were 11.42 ± 3.87 μm² and 37.6 ± 9.90 μm², respectively. When HA was blended with PVP, the pore area decreased as the HA concentration increased from 1% *w*/*w* to 3% *w*/*w*. Specifically, the values were 21.68 ± 4.86 μm² and 7.53 ± 3.86 μm², respectively. When HA-Gly-OH was blended with PVP, instead, the pore area increased with the concentration. Specifically, values of 11.31 ± 4.26 μm² and 30.19 ± 3.56 μm² were observed for PVP-HA-Gly-OH 1% and PVP-HA-Gly-OH 3%, respectively. Although the porosity values are in good agreement with the literature on electrospun scaffolds for wound healing applications [51], the pore sizes observed in this study are below the optimal threshold for deep cellular infiltra-

tion; they fall within a range that is particularly suitable for controlled drug delivery applications [52]. However, for proposing the herein discussed electrospun scaffolds as wound dressing, a water vapor transmission rate measurement remains a crucial parameter to evaluate. It is well known that the absence of this test could be a limitation.

To investigate the morphology of the bilayer PDLLA/PVP HA-derived electrospun scaffolds, with particular attention to the layer thickness, cross-sections were imaged by SEM (Figures S5–S9), and the data has been reported in Table 3. This approach was also applied in experiments where cell cultures on bilayer scaffolds had hydrophilic and hydrophobic sides in order to discern better adhesion and integration over one of the two sides of the electrospun scaffold. In general, it is well established that cells preferentially adhere to hydrophilic layers [53]. Not only is cross-sectional analysis commonly used to investigate the internal morphology of a material, offering a direct magnified observation of interfaces, layer thickness, and potential subsurface defects, but also to investigate interfacial adhesion and identify microscopic delamination of the two layers. In this work, the two layers were electrospun on the same day to avoid interfacial delamination. Preliminary observations showed that delamination occurred when the bilayer scaffolds were fabricated sequentially over two consecutive days (Figure S10).

Table 3. Mean layer thickness (± standard deviation) of bilayer electrospun scaffolds.

Scaffold	l_{PDLLA} (μm)	l_{PVP} (μm)	$l_{PVP\text{-}HA\ 1\%}$ (μm)	$l_{PVP\text{-}HA\ 3\%}$ (μm)	$l_{PVP\text{-}HA\text{-}Gly\text{-}OH\ 1\%}$ (μm)	$l_{PVP\text{-}HA\text{-}Gly\text{-}OH\ 3\%}$ (μm)
PDLLA/PVP	241.15 ± 8.51	312.26 ± 15.29	-	-	-	-
PDLLA/PVP-HA 1%	420.29 ± 15.04	-	309.57 ± 31.10	-	-	-
PDLLA/PVP-HA 3%	526.14 ± 10.59	-	-	341.57 ± 32.91	-	-
PDLLA/PVP-HA-Gly-OH 1%	168.57 ± 5.91	-	-	-	222.57 ± 13.59	-
PDLLA/PVP-HA-Gly-OH 3%	217.86 ± 6.77	-	-	-		85.04 ± 5.18

3.3. Water Contact Angle Measurements

To evaluate changes in the wettability of PVP scaffolds after HA-glycine conjugation, static water contact angle (SWCA) measurements were performed. The results are shown in Figure 5, Figure S11, and Table S1. As shown in Table S1, the single-layer PDLLA scaffold exhibited a contact angle of 131.50 ± 10.71°, confirming the intrinsic hydrophobic character of the polymer. In contrast, the PVP surface displayed a markedly lower contact angle of 57.07 ± 17.51°, indicating that the introduction of PVP significantly decreased the hydrophobicity of the scaffold. When HA was incorporated into the PVP layer at a concentration of 3% (*w*/*w*), the contact angle further decreased to 36.75 ± 19.41°, suggesting an enhancement in surface hydrophilicity. This trend is consistent with previous studies on HA-coated electrospun scaffolds, which reported the increasing HA content generally leads to more hydrophilic surfaces due to the highly polar nature of HA [54]. Interestingly, when HA-Gly-OH was used as an additive in the PVP layer at the same concentration (3% *w*/*w*), a significant increase in SWCA was observed (128.20 ± 12.61°), indicating a more hydrophobic apparent surface behavior. This result may be related to changes in surface organization and fiber morphology induced by the modified HA derivative, which can influence how water droplets interact with the scaffold surface. It should also be considered that electrospun mats are highly porous and typically exhibit considerable surface roughness. Under these conditions, the ap-

parent contact angle is not determined solely by surface chemistry but can also be strongly affected by the fibrous architecture and by the presence of air pockets trapped within the scaffold. These morphological features can lead to deviations from intrinsic wettability of the materials, often resulting in higher apparent contact angles. In addition, this behavior may be partially associated with the shrinkage of the PVP-HA-Gly-OH 3% layer on the PDLLA substrate after processing. This effect, suggested by the reduced thickness of the electrospun layer (Table 3), may lead to a lower effective surface coverage on the top layer. In the bilayer configuration, this could expose a larger fraction of the intrinsically hydrophobic–PDLLA substrate, thereby increasing its contribution to the measured contact angle. Overall, the trends observed here are consistent with previous studies on PCL scaffolds fabricated by-melt-extrusion 3D printing and subsequently functionalized for conjugation with HA-glycine peptides, where surface architecture and coverage were also reported to influence the apparent wettability [33].

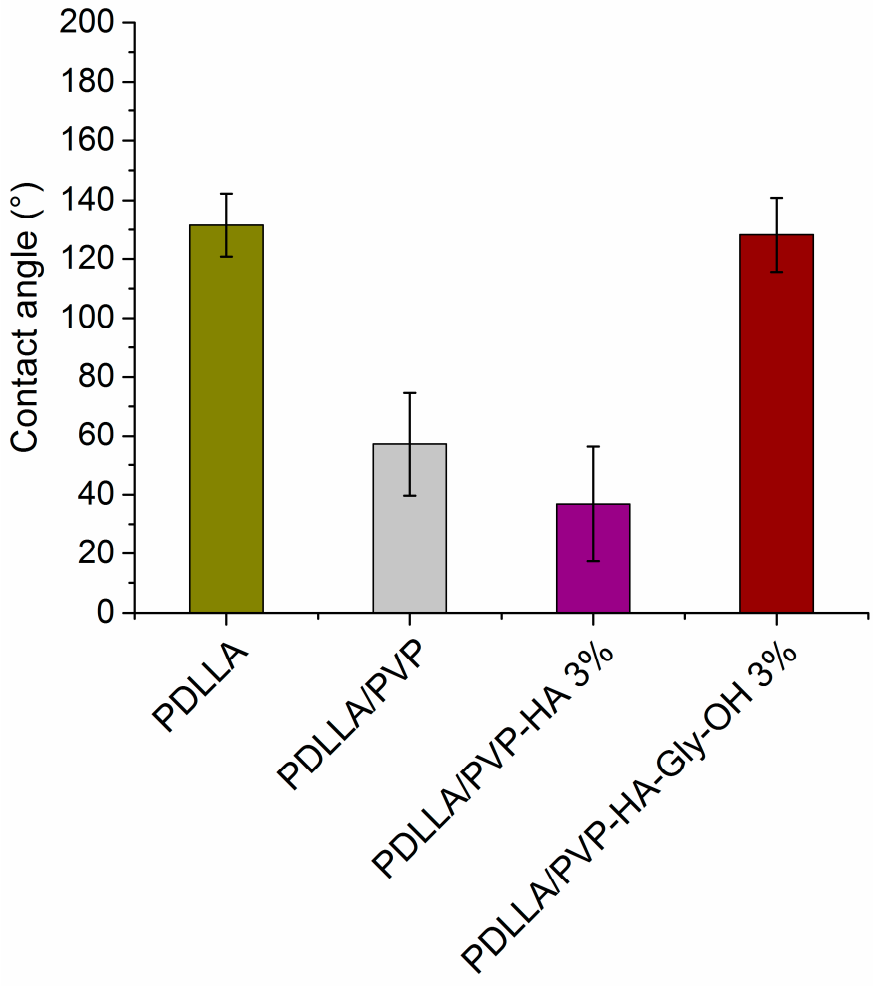

Figure 5. Mean contact angle values (±standard deviation) for electrospun mats of PDLLA, PDLLA/PVP, PDLLA/PVP-HA 3%, and PDLLA/PVP-HA-Gly-OH 3%.

3.4. Mechanical Properties of Electrospun Composites

Figure 6 and Table S2 show the Young's modulus of the electrospun composite materials, calculated by statistically analyzing over 300 force-distance curves for each sample. Although each distribution corresponds to a single scaffold formulation, the measurements were collected from multiple independent AFM acquisitions performed across different regions of the electrospun substrates (Figure 7). Consequently, the re-

ported standard deviations mainly reflect intrinsic spatial heterogeneity of the samples. This extensive data collection enhances the accuracy and reproducibility of the mechanical properties' evaluation and accounts for the inherent heterogeneity and anisotropy of the fibrous network, providing a robust characterization of the composite's elastic properties.

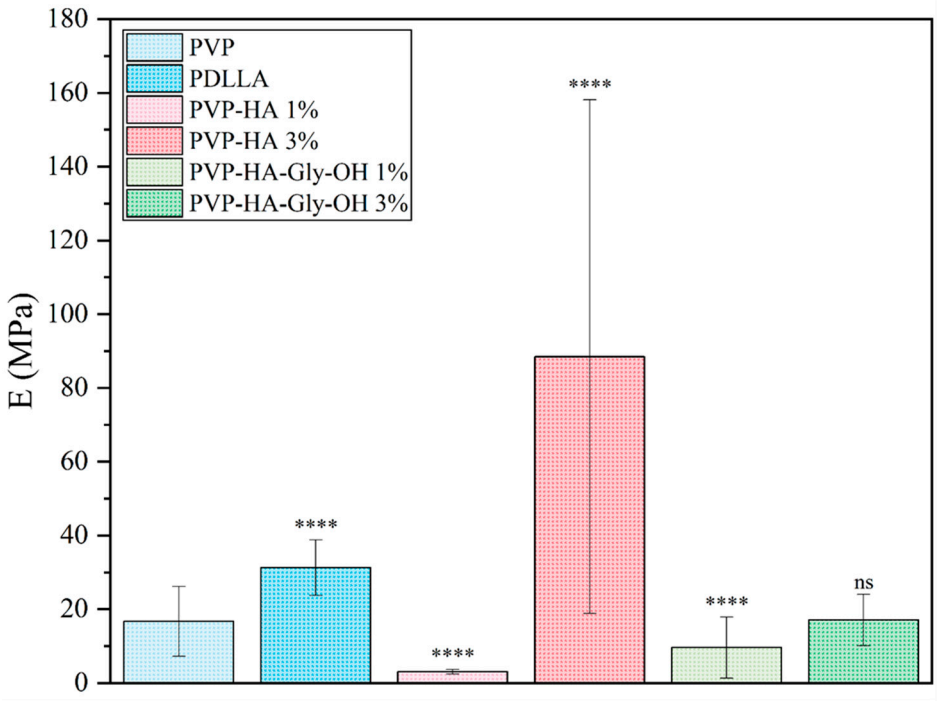

Figure 6. Mean Young's modulus values (±standard deviation) for electrospun mats of PVP, PDLLA, and their blends with HA or HA-Gly-OH at different concentrations (n = 300 per group). Asterisks indicate the level of statistical significance among groups (ns, not significant; ****, $p < 0.0001$) with PVP as reference sample. All the statistical comparison results are reported in Table S2.

The results clearly demonstrate distinct mechanical behaviors between the internal and external layers of the material. Specifically, PVP fibers, which constitute the internal layer, exhibit a significantly lower Young's modulus compared to the external layer composed of PDLLA fibers. Quantitatively, the Young's modulus of the PVP fibers is approximately half that of the PDLLA fibers, indicating a much lower stiffness and a higher degree of flexibility.

The mixed solution of HA and PVP induces notable changes in the mechanical properties of the resulting electrospun fibers, with the effect strongly dependent on the concentration of HA present in the blend. At low HA content (1% *w*/*w*), a pronounced reduction in Young's modulus was observed in comparison to fibers composed of pure PVP. This behavior could be attributed to the ability of HA chains to disrupt interchain interactions among PVP molecules. Specifically, the introduction of HA increases the free volume within the polymer network, as confirmed by diameter dimensions, and enhances the hydrophilicity of the system, leading to a more hydrated and loosely packed fiber structure [55,56].

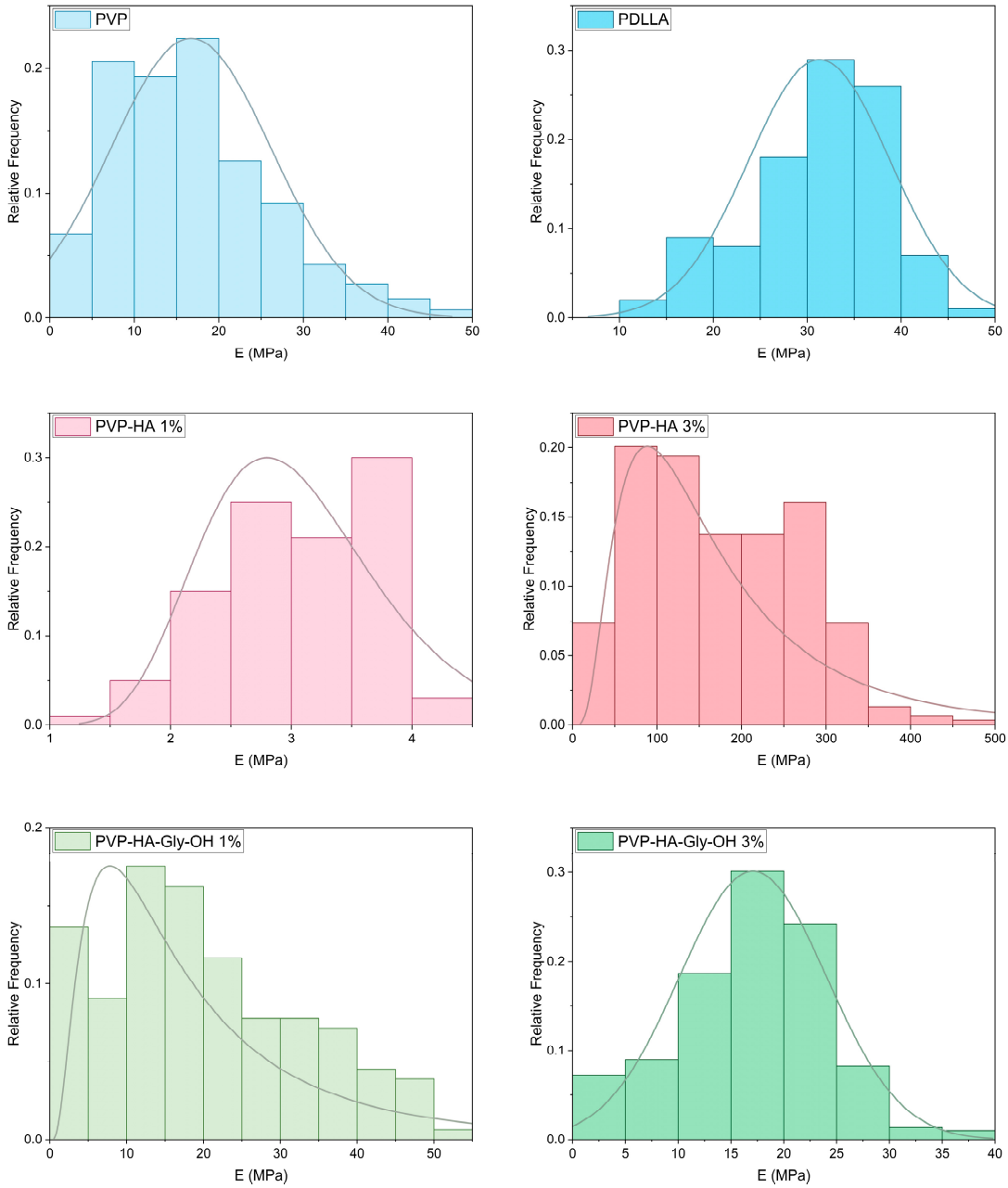

Figure 7. Histogram of electrospun scaffolds Young Modulus (E) distributions for pristine PVP, pristine PDLLA, PVP-HA 1%, PVP-HA 3%, PVP-HA-Gly-OH 1%, and PVP-HA-Gly-OH 3%. Every distribution is based on 300 acquisitions.

These morphological changes collectively contribute to a reduction in overall stiffness, i.e., the fibers become softer and less cohesive. Interestingly, when the HA concentration increases to 3% *w*/*w*, an inverse trend can be observed: the modulus increases significantly, albeit with a high degree of variability. This suggests that at higher loadings, HA no longer acts as a simple softening component, but it likely induces the formation of localized, HA-rich microdomains within the fibrous matrix. These microdomains act as rigid inclusions under mechanical load, thereby increasing the stiffness of the composite fibers. However, the heterogeneous distribution of soft and stiff domains results in mechanical inconsistency, which is reflected in the variability of the measured modulus values as suggested by mean standard deviation values (±69.65). Such behavior is consistent with reports on other polymer blends containing polysaccharides, in which phase separation and microstructural heterogeneity lead to complex mechanical re-

sponses [57]. As further support for this finding, the datasets exhibit asymmetric distributions. Statistical analysis was performed to evaluate differences in the Young's modulus among the various sample groups. Initially, a one-way analysis of variance (ANOVA) was conducted to assess whether overall differences existed between formulations. Considering the potential heterogeneity of variance among groups, pairwise comparisons were subsequently performed using Welch's *t*-test, which does not assume homogeneity of variances and is therefore more suitable for this dataset. This combined approach allowed us to identify both the overall effect of formulation on mechanical properties and the specific differences between individual groups with a high degree of statistical robustness.

The conjugation of Gly-OH to HA significantly alters the mechanical response of the fiber system. At a lower concentration (HA-Gly-OH 1% *w*/*w*), the Young's modulus increases compared to the PVP-HA 1% formulation, yet it remains substantially lower than that of bare PVP fibers. This indicates that Gly-OH conjugation helps to restore the network's coherent structure, providing limited reinforcement of the polymer matrix. Because Gly-OH contains reactive groups that can interact electrostatically and generate hydrogen bonds with both PVP and HA, its presence decreases chain mobility and increases interfacial adhesion. The resulting network is more compact and uniformly connected, somewhat offsetting the stiffness reduction caused by HA at low concentrations. In contrast, when the HA concentration increases, i.e., HA-Gly-OH 3% *w*/*w*, the mechanical behavior shifts markedly.

The Young's modulus reaches that of bare PVP, and no statistically significant difference was observed. This result implies that Gly-OH effectively prevents the formation of rigid, HA-rich microdomains typically associated with high HA content, thereby promoting a more uniform and homogeneous phase distribution within the fiber network. Gly-OH enhances the uniform distribution of HA within the PVP matrix, minimizing local stress peaks and resulting in a steadier and more consistent mechanical behavior. In general, these results indicate that Gly-OH functions as a network modifier. Its presence optimizes the chemical and physical interactions between PVP and HA, adding binding motifs that enhance miscibility and interfacial compatibility. As a result, the rigidity of the fibers can be modified by simultaneously managing the HA concentration and Gly-OH content, leading to materials with tunable and reproducible mechanical properties. This interpretation is consistent with earlier research demonstrating that covalent functionalization or modification of pendant groups on HA greatly influences the viscoelastic and mechanical properties of hybrid networks [58–60]. Statistical analysis confirms that the Young's modulus of the electrospun mats is significantly influenced by both HA concentration and the presence of Gly-OH, as demonstrated by a two-way ANOVA ($p \ll 0.001$). The pairwise comparisons reveal highly significant differences among most formulations (****), with the only exception being the comparison between bare PVP and PVP–HA–Gly-OH 3%, which do not reach statistical significance. This further supports the observation that Gly-OH conjugation at higher HA concentrations effectively restores the mechanical properties to levels comparable with the unmodified polymer.

The pronounced difference in mechanical properties is crucial for applications requiring a gradient in mechanical performance, such as in layered scaffolds for tissue engineering, where the mechanical mismatch can be tailored to mimic the native tissue architecture or to enhance the integration between layers.

In this context, the local Young's modulus values measured by AFM nanoindentation for the present electrospun scaffolds fall within the broad range reported for skin and skin-mimicking materials at comparable scales. The elastic properties of native human skin span a very wide range depending on anatomical location, hydration state, age,

and, most importantly, on the measurement technique and length scale considered. Reported Young's modulus values range from a few kPa to several tens, or even over one hundred MPa, reflecting the highly anisotropic and viscoelastic nature of skin tissue. For instance, suction-based measurements typically yield elastic moduli in the range of approximately 0.05–0.15 MPa, torsional tests report values around 0.4–0.9 MPa, while uniaxial tensile tests on excised skin commonly result in Young's modulus values between 4 and 20 MPa [61,62]. At smaller length scales or under localized indentation, higher apparent moduli—reaching several tens of MPa—have also been reported [61,63]. Overall, this mechanical compatibility, combined with the bilayer architecture, suggests that the developed scaffolds are particularly suitable for superficial and partial-thickness wounds, where conformability, flexibility, and local mechanical cues supporting fibroblast activity are critical.

3.5. Evaluation of Cytocompatibility of Electrospun Scaffolds

The cytocompatibility of single/double-layer electrospun scaffolds was evaluated by assessing L929 fibroblast viability at 24 and 48 h post-seeding. Untreated cells served as the control group, with viability normalized to 100% (Figure 8).

Cells cultured on PVP-only scaffolds exhibited a slight but statistically significant reduction in cell viability at 24 h (** $p < 0.01$). while no significant difference was observed. However, this effect was no longer evident at 48 h, suggesting a transient cytotoxic response that may be mitigated over time as cells adapt to the scaffold microenvironment. In contrast, PDLLA scaffolds, widely employed in biomedical applications due to their biodegradability and mechanical strength, showed no statistically significant difference in cell viability compared to untreated cells at either time point, confirming their acceptable biocompatibility. Scaffolds incorporating 1% *w*/*w* hyaluronic acid (PVP-HA 1%) maintained viability levels significantly higher than untreated cells at both time points, highlighting HA's contribution to scaffold biocompatibility. HA is known to support cell adhesion and proliferation through interactions with CD44 receptors and its hydrophilic nature, which improves scaffold hydration and mimics ECM properties, thereby creating a favorable environment for fibroblast growth [64]. Interestingly, increasing the HA concentration to 3% *w*/*w* (PVP-HA 3%) resulted in a significant decrease in cell viability (** and °° $p < 0.01$), suggesting that excessive HA may disrupt scaffold architecture or osmotic balance, thereby impairing cell–material interactions [23,65]. Similar trends have been reported in literature, where high HA content led to scaffold swelling and reduced mechanical integrity, ultimately compromising cellular compatibility [66]. The addition of Gly-OH to HA-modified scaffolds significantly enhanced cell viability at both time points. PVP-HA-Gly-OH 1% scaffolds showed the highest cell proliferation, even surpassing untreated cells. Rather than acting as a cell-adhesion motif, glycine is more likely to influence scaffold performance through its physicochemical properties. As a small zwitterionic amino acid, glycine can act as a humectant and plasticizer, improving the moisture retention, flexibility, and hydrophilicity of the scaffold. These features help stabilize the membrane structure, reduce cytotoxic stress, and facilitate nutrient exchange, thereby indirectly supporting cell growth. This interpretation is consistent with previous studies demonstrating that bioactive additives can modulate scaffold hydration and mechanical behavior to enhance biocompatibility. For instance, Pepe et al. highlighted how chemical modifications in HA-based electrospun scaffolds and highlighted the role of functional groups in enhancing cell adhesion and proliferation by improving hydrophilicity and mimicking the ECM-like environment, promoting cell adhesion and proliferation [23]. Additionally, Niu and Galluzzi demonstrated that HA/collagen nanofiber scaffolds support endothelial cell proliferation and phenotypic maintenance due to HA's physicochemical properties [67].

Although PVP-HA-GlyOH 3% scaffolds also showed increased viability compared to PVP-HA 3% alone, they remained significantly lower than untreated cells, suggesting that glycine's beneficial effects may be limited when paired with higher HA concentrations. These results reinforce the importance of balanced scaffold composition. The PVP-HA-GlyOH 1% formulation consistently demonstrated superior cytocompatibility and was therefore selected for further development in bilayer scaffold design.

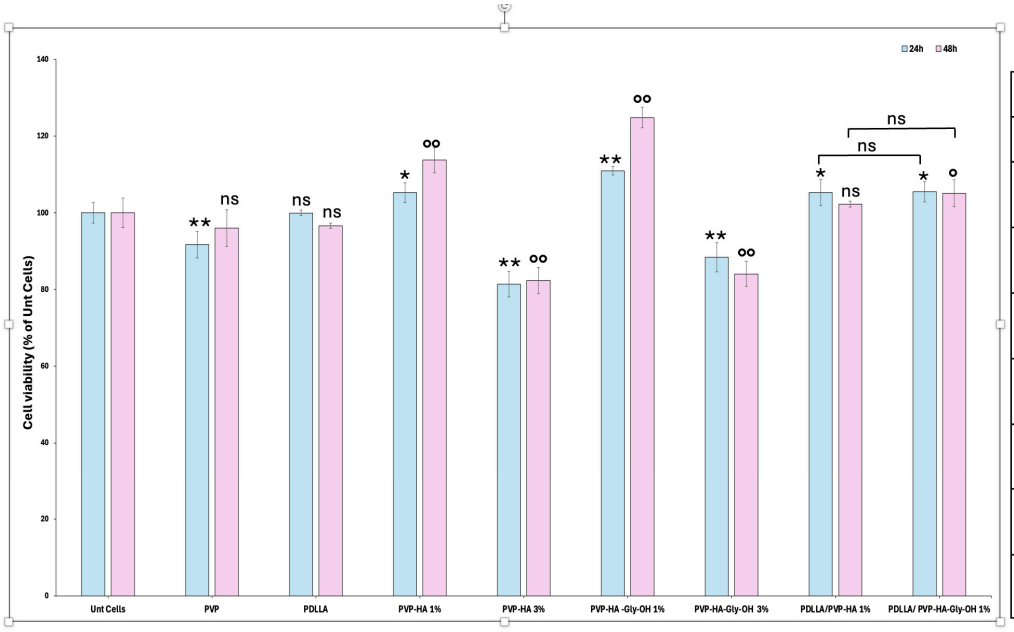

	24h	48h
Unt Cells vs PVP	**p<0.01	ns
Unt Cells vs PDLLA	ns	ns
Unt Cells vs PVP-HA 1%	*p<0.05	°°p<0.01
Unt Cells vs PVP-HA 3%	**p<0.01	°°p<0.01
Unt Cells vs PVP-HA Gly-OH 1%	**p<0.01	°°p<0.01
Unt Cells vs PVP-HA-Gly-OH 3%	**p<0.01	°°p<0.01
Unt Cells vs PDLLA/PVP-HA 1%	*p<0.05	ns
Unt Cells vs PDLLA/ PVP-HA -Gly-OH 1%	*p<0.05	°p<0.05
PDLLA/PVP-HA 1% vs PDLLA/ PVP-HA-Gly-OH 1%	ns	ns

Figure 8. Cell viability of L929 fibroblasts cultured on various electrospun scaffold formulations at 24 and 48 h. Bar graph showing cell viability (% of untreated cells) for seven treatment groups: Untreated Cells, PVP, PDLLA, PVP-HA 1%, PVP-HA 3%, PVP-HA-Gly-OH 1%, and PVP-HA-Gly-OH 3%-, PDLLA/PVP-HA1%, and PDLLA/PVP-HA-Gly-OH 1%. Blue bars represent viability at 24 h; pink bars represent viability at 48 h. Error bars indicate standard deviation. Statistical significance is denoted as follows: ** and °° $p < 0.01$, * and ° $p < 0.05$, and ns = not significant.

Cells cultured on PDLLA/PVP-HA1% scaffolds exhibited viability levels comparable to untreated cells at both time points, with no statistically significant differences observed at 48 h (ns). This suggests that the combination of PDLLA and 1% *w*/*w* of hyaluronic acid provides a biocompatible environment favorable to cell survival. PDLLA is widely recognized for its biodegradability and mechanical strength, while HA contributes to scaffold hydration and cell–matrix interactions, making this blend suitable for biomedical applications [66].

In contrast, the PDLLA/PVP-HA-Gly-OH 1% scaffolds demonstrated a statistically significant increase in cell viability at both 24 h (* $p < 0.05$) and 48 h (° $p < 0.05$). However, no significant differences were observed when compared to the PDLLA/PVP-HA 1% scaffolds at either time point. This enhancement indicates a synergistic effect between HA and Gly-OH, where glycine likely improves moisture retention and scaffold flexibility, thereby promoting membrane stability and reducing oxidative stress [68]. The sustained increase in viability over time suggests that the bilayer structure not only supports initial cell attachment but also facilitates ongoing proliferation.

These findings are consistent with previous studies showing that bilayer electrospun scaffolds can mimic the extracellular matrix and provide a favorable microenvironment for cell growth. For instance, Petrova et al. demonstrated that bilayer chitosan/alginate scaffolds enhanced mesenchymal stem cell proliferation due to their high porosity and layered architecture [66]. Similarly, Mohammadalizadeh et al. emphasized

the importance of blending synthetic and natural polymers to improve scaffold biocompatibility and mechanical performance [68]. Overall, the PDLLA/PVP-HA-Gly-OH 1% formulation emerged as the most promising candidate for further development, offering superior cytocompatibility and potential for tissue engineering applications.

To further assess the cytocompatibility of the bilayer electrospun scaffolds, live/dead staining was performed using Calcein AM and BOBO-3 Iodide to visualize viable and non-viable L929 fibroblasts, respectively (Figure 9). Both scaffold formulations, PDLLA/PVP-HA 1% and PDLLA/PVP-HA-Gly-OH 1%, exhibited strong green fluorescence with minimal red signal, comparable to untreated cells, confirming high cell viability across all conditions. Cells appeared well spread and uniformly distributed, indicating favorable scaffold architecture and optimal culture conditions. Notably, the PDLLA/PVP-HA-Gly-OH 1% scaffold demonstrated a slightly more pronounced enhancement in cell viability relative to PDLLA/PVP-HA 1% alone. This suggests that the incorporation of glycine may have beneficially influenced the scaffold's physicochemical properties. These modifications are critical for promoting cell adhesion, reducing oxidative stress, and maintaining integrity during culture. Enhanced wettability and porosity resulting from glycine incorporation may also facilitate nutrient diffusion and waste removal, further supporting cell survival and proliferation. These observations align with previous findings that glycine-modified electrospun scaffolds can improve cellular responses by mimicking native ECM characteristics and enhancing biocompatibility. For instance, Niemczyk-Soczynska et al. highlighted that hydrophilic surface functionalization of electrospun nanofibers significantly improves cell adhesion and proliferation by enhancing bioactivity and ECM mimicry [69]. Additionally, Ruccolo et al. reviewed the role of electrospun bio-scaffolds in promoting mesenchymal stem cell differentiation, emphasizing the importance of scaffold surface chemistry and architecture in modulating cell behavior [70]. Furthermore, El-Ghoul et al. reported that bioactive additives in electrospun scaffolds, such as natural compounds and amino acids, can enhance wound healing and cellular compatibility by improving scaffold hydrophilicity and mechanical properties [71].

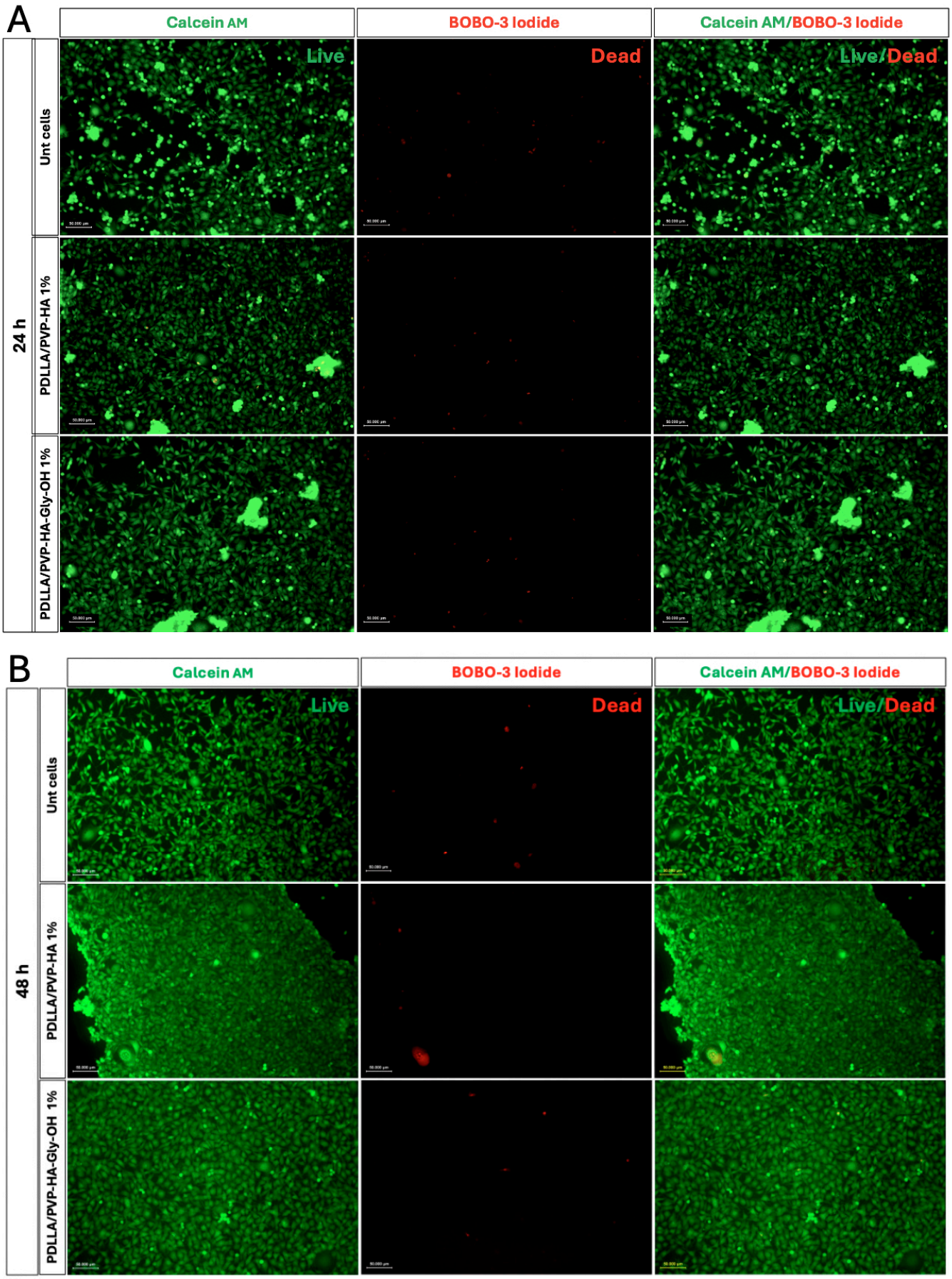

Figure 9. Live/dead fluorescence imaging of L929 fibroblasts cultured on bilayer electrospun scaffolds. Representative fluorescence microscopy images showing cell viability after 24 h (panel

(**A**)) and 48 h (panel (**B**)), under three conditions: Untretated cells (control), PDLLA/PVP-HA 1%, and PDLLA/PVP-HAGly-OH 1%. Columns display staining with Calcein AM (green, viable cells), BOBO-3 Iodide (red, non-viable cells), and merged images.

Taken together, the fluorescence imaging results reinforce the quantitative viability data and confirm that the PDLLA/PVP-HA-Gly-OH 1% bilayer scaffold offers a more favorable microenvironment for fibroblast growth. This formulation holds promise for further development in tissue engineering applications where scaffold biocompatibility and cellular integration are crucial.

3.6. Sol (SF) and Gel Fraction (GF)

SF and GF were calculated to evaluate the stability of the individual electrospun layers and the material loss following immersion in an aqueous environment. This analysis allows the distinction between the soluble fraction (sol fraction), consisting of non-crosslinked or weakly bound material released into the solution, and those insoluble fraction (gel fraction), which represents the stable polymeric network responsible for maintaining the structural integrity of the scaffold.

As reported in Table 4, PVP, PVP-HA 1%, and PVP-HA-Gly-OH 1% displayed SF values of 42 ± 16%, 57 ± 5%, and 30% ± 5%, respectively. Statistical analysis, including one-way ANOVA followed by Tukey's post-hoc test, revealed significant differences among the different scaffold types (Figure 10). In particular, PVP-HA 1% showed a significantly higher material loss compared to pure PVP, with a statistically significant difference (**, $p < 0.01$). This result indicates reduced stability of HA-containing scaffolds in aqueous environments.

Table 4. Mean sol and gel fraction values (±standard deviation).

Scaffold	Sol-Fraction (%)	Gel Fraction (%)
PVP	42 ± 16	58 ± 16
PVP-HA 1%	57 ± 5	43 ± 5
PVP-HA-Gly-OH 1%	30 ± 5	71 ± 5

In contrast, PVP-HA-Gly-OH 1% exhibited the lowest sol fraction, resulting in significantly higher stability compared to both PVP scaffolds (* and $p < 0.05$) and PVP-HA 1% *w*/*w* scaffolds (****, $p < 0.0001$). Consequently, GF values were 58 ± 16%, 43% ± 5%, and 71% ± 5% for the same type of scaffolds. The data obtained for PVP are in agreement with results published by Catalani and co-workers [72], as well as the values obtained for PVP-HA 1% could be associated with the hydrophilicity of native polysaccharide. Surprisingly, the behavior of PVP-HA-Gly-OH 1% suggests that functionalization of hyaluronic acid with glycine contributes to improving material stability by reducing dissolution in aqueous environments. It is important to acknowledge that the conditions employed for sol and gel fraction calculations are to be regarded as initial screening. However, to overcome this limitation and to confirm the degradation behavior in a more physiological environment, such as in phosphate buffer solution, future analyses are necessary.

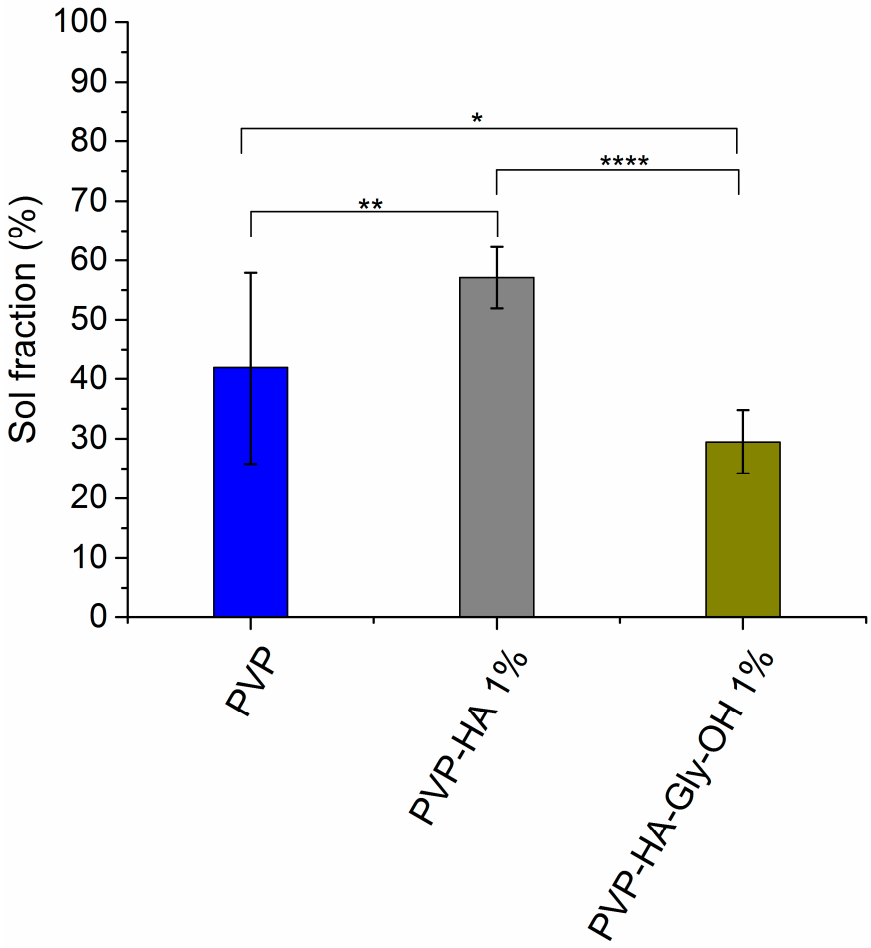

Figure 10. Mean sol-fraction values (± standard deviation) for electrospun scaffolds of PVP, PVP-HA 1%, and PVP-HA-Gly-OH 1%. Asterisks indicate the level of statistical significance among groups (*, $p < 0.05$; **, $p < 0.01$; ****, $p < 0.0001$).

3.7. Cumulative Release

The cumulative release of HA and HA-Gly-OH was investigated by UV−Vis spectroscopy in a pH 5.5 sodium acetate solution at 570 nm. The cumulative drug release was expressed in terms of percentage according to a convenient calibration curve and showed values compatible between PVP-HA 1% and PVP-HA-Gly-OH 1%. The maximum degree of release was obtained after 2 h, when PVP-HA 1% and PVP-HA-Gly-OH 1% displayed percentages of 15 ± 4% and 14 ± 2%, respectively. Moreover, a nearly linear sustained release was observed from 4 h to 24 h (Figure 11), where the absorbance value reached a plateau.

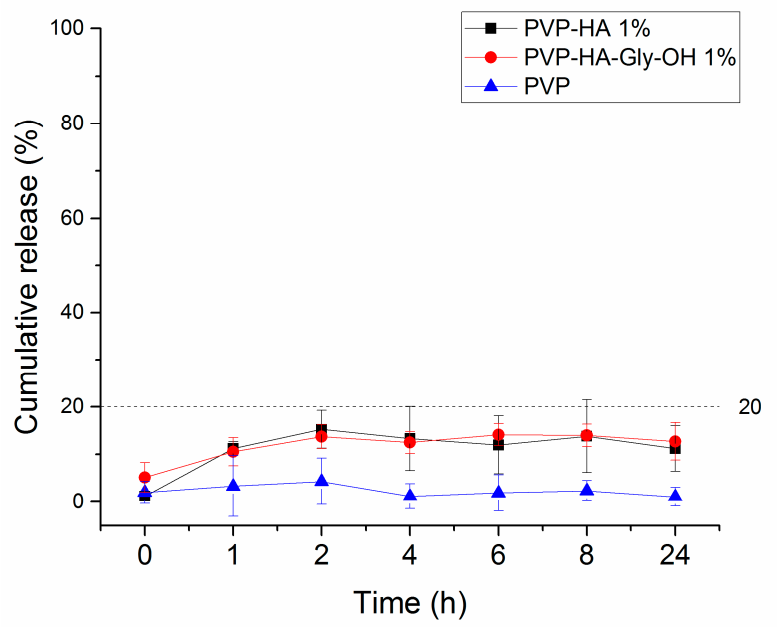

Figure 11. Cumulative release (±standard deviation) of HA, HA-Gly-OH and PVP from 0 to 24 h.

The rate of both HA and HA-Gly-OH release is hypothesized to be related to entrapped native and semi-synthetic polysaccharides within the polymer network of the crosslinked electrospun scaffold, providing resistance to the diffusion out of the swollen matrix. It is worth noting that during the photochemical crosslinking of the electrospun scaffolds, a reaction between PVP and both HA and HA-Gly-OH may occur, potentially reducing their cumulative release. This phenomenon has been observed during the UV irradiation of chitosan/PVP blends, where polysaccharide hydroxyl radicals can react with PVP to form a crosslinked structure [73].

After the cumulative release, the presence of hyaluronic acid within PVP-HA 1% fibers has been qualitatively evaluated by the phenol colorimetric assay. The scaffolds have been suspended in water, then treated with a 5% aqueous phenolic solution and concentrated sulfuric acid. Finally, the absorbance was measured at 490 nm. As it can be seen in Figure S12, the sample containing HA is characterized by a yellow-brown solution, different from the PVP sample and the blank. This color is attributed to HA that is still present within the fibers and that could be available after a degradation. Moreover, a further evaluation of HA presence within the fibers, the cumulative release, was conducted on an uncrosslinked PVP-HA 1% electrospun scaffold. In this case, the maximum degree of release was obtained after 1 h, where a percentage of 85 ± 2% was observed. (Figure S13). It is worth noting that this analysis has been performed in pH 5.5 acetate buffer, providing a relevant proof-of-concept for the intended application. However, the medium does not fully replicate the complex ionic composition of a physiological environment. Therefore, future release studies in phosphate buffer solution are needed to confirm the release profile.

4. Conclusions

This study reports the successful fabrication and characterization of an electrospun bilayer wound dressing system, consisting of an external PDLLA layer and an internal PVP-based layer incorporating either native HA or semi-synthetic HA-Gly-OH at concentrations of 1% and 3% *w*/*w*. While bilayer scaffolds electrospun on different days delaminated, they maintained their integrity when electrospun on the same day. The cross section imaged by SEM reveals intimate interfaces between PDLLA and PVP layers with achieved thickness, suggesting the absence of layer mixing. Sol-gel testing on photo-

chemically crosslinked scaffolds proved the stability in aqueous solution of the scaffolds, which is functional to the obtention of the slow release of hyaluronic acid tested at the maximum level of 20%. Mechanical testing revealed distinct behaviors between the two layers, with both native HA and HA-Gly-OH significantly modulating scaffold stiffness in a concentration-dependent manner. Biocompatibility assays demonstrated that while each layer was individually compatible with fibroblasts, higher concentrations of HA and HA-Gly-OH induced a dose-dependent cytotoxic response. Based on these findings, formulations containing 1% *w*/*w* of polysaccharide additives were selected for bilayer scaffold development. Notably, the PDLLA/PVP-HA-Gly-OH 1% bilayer demonstrated increased cell viability, highlighting the beneficial role of glycine in improving scaffold physicochemical properties and supporting cellular responses. Overall, the results highlight the potential of this bilayer electrospun system for application as a medical device. Future *in vitro* and *in vivo* studies are required to further validate its therapeutic efficacy, biocompatibility, and long-term stability under physiological conditions.

Supplementary Materials: The following supporting information can be downloaded at: https://www.mdpi.com/article/10.3390/polysaccharides7020046/s1, Figure S1: ^{1}H-NMR spectrum of HA-Gly-OEt in D_2O; Figure S2: ^{1}H-NMR spectrum of HA-Gly-OH in H_2O/D_2O 9:1 *v*/*v*; Figure S3: Fibers diameter distribution for neat PVP, neat PDLLA, PVP-HA 1%, PVP-HA 3%, PVP-HA-Gly-OH 1%, and PVP-HA-Gly-OH 3% electrospun scaffolds; Figure S4: Pore area distribution for neat PVP, neat PDLLA, PVP-HA 1%, PVP-HA 3%, PVP-HA-Gly-OH 1%, and PVP-HA-Gly-OH 3% electrospun scaffolds; Figure S5: Cross-section SEM images of PDLLA/PVP bilayer electrospun scaffolds; Figure S6: Cross-section SEM images of PDLLA/PVP-HA 1% bilayer electrospun scaffolds; Figure S7: Cross-section SEM images of PDLLA/PVP-HA 3% bilayer electrospun scaffolds; Figure S8: Cross-section SEM images of PDLLA/PVP-HA-Gly-OH 1% bilayer electrospun scaffolds; Figure S9: Cross-section SEM images of PDLLA/PVP-HA-Gly-OH 3% bilayer electrospun scaffolds; Figure S10: Effect of electrospinning timing on delamination of bilayer electrospun scaffolds; Figure S11: Contact angle measurement for neat PDLLA, PDLLA/PVP, PDLLA-PVP-HA 3%, and PDLLA-PVP-HA-Gly-OH 3%; Table S1: Contact angle values for neat PDLLA, PDLLA/PVP, PDLLA/PVP-HA 3%, and PDLLA/PVP-HA-Gly-OH 3%; Table S2: Young's Modulus (E) values of the electrospun scaffolds; Table S3: Pairwise statistical comparisons of Young's modulus values; Figure S12: Phenol assay results for PVP and PVP-HA 1% electrospun scaffolds; Figure S13: Cumulative release of HA from uncrosslinked PVP-HA 1% electrospun scaffolds.

Author Contributions: A.L., F.A., M.C. K.S.-L.: Investigation, methodology, data curation, and writing—original draft; L.F., S.M., P.C., and I.I.: Methodology, writing—original draft; G.D.L.: writing—review and editing; G.M.L.M., G.C.: Conceptualization, formal analysis, writing—review and editing, funding acquisition and resources; A.P., and B.B.: Conceptualization, project administration, supervision, resources, funding acquisition, and writing—review and editing. All authors have read and agreed to the published version of the manuscript.

Funding: This work was supported by Ecosistema di Innovazione "Rome Technopole" funded by MUR—Spoke 3-University education, industrial PhD courses, internationalization. Project BEST-DRESS—Biomimetic Electrospun Scaffold as susTainable wound DRESSing device, CUP F33C24000360006, ECS_0000024 Rome Technopole—PNRR Mission 4, Component 2, Investment 1.5, funded by the European Union—NextGenerationEU.

Institutional Review Board Statement: Not applicable.

Data Availability Statement: The original contributions presented in this study are included in the article/supplementary material. Further inquiries can be directed to the corresponding authors.

Acknowledgments: The authors thank Tania Ruspandini and the Laboratory of Electron Microscopy and Microanalysis of the Department of Earth Sciences, Sapienza University of Rome, for the SEM analysis, performed with FEI Quanta 400 high resolution field ESEM instrument. The authors thank Alessandro Laurita of the Department of Basic and Applied Sciences, University of Basilicata for the cross-section analyses performed with Philips-FEI ESEM XL30-LaB6 instrument.

Conflicts of Interest: The authors declare no conflicts of interest.

Abbreviations

The following abbreviations are used in this manuscript:

AFM	Atomic force microscopy
ATCC	American Type Culture Collection
ATR-FT-IR	Attenuated total reflectance Fourier transform infrared spectroscopy
CTAB	Cetyltrimethyl ammonium bromide
DMEM	Dulbecco's Modified Eagle Medium High Glucose
DMSO	Dimethylsulfoxide
DMT	Derjaguin–Muller–Toporov
DS	Degree of substitution
DSS	3-(Trimethylsilyl)propionic-2,2,3,3-d_4 acid sodium salt
ECM	Extracellular matrix
EDC·HCl	*N*-(3-(Dimethylamino)propyl)-*N*′-ethylcarbodiimide hydrochloride
FBS	Fetal bovine serum
GAGs	Glycosaminoglycans
GlcA	D-glucuronic acid
GlcNAc	*N*-acetyl-D-glucuronic acid
Gly-OEt·HCl	Glycine ethyl ester hydrochloride
HA	Hyaluronic acid
HFP	1,1,1,3,3,3-Hexafluoro-2-propanol
MES	2-(*N*-Morpholino)ethanesulfonic acid hydrate
MTT	3-(4,5-dimethylthiazol-2-yl)-2,5-diphenyltetrazolium bromide
NaCl	Sodium chloride
NaOH	Sodium hydroxide
NMR	Nuclear magnetic resonance
PBS	Phosphate-buffered saline
PDLLA	Poly-D,L-lactide
PSA	Penicillin/streptomycin/amphotericin B
PVP	Polyvinylpirrolidone
SEM	Scanning electron microscopy
SWCA	Static water contact angle
s-NHS	*N*-Hydroxysulfosuccinimide sodium salt
UPW	Ultra-pure water

References

1. Byrd, A.L.; Belkaid, Y.; Segre, J.A. The human skin microbiome. *Nat. Rev. Microbiol.* **2018**, *16*, 143–155.
2. Kabashima, K. Overview: Immunology of the Skin. In *Immunology of the Skin: Basic and Clinical Sciences in Skin Immune Responses*; Kabashima, K., Ed.; Springer: Tokyo, Japan, 2016; pp. 1–11.
3. Takeo, M.; Lee, W.; Ito, M. Wound healing and skin regeneration. *Cold Spring Harb. Perspect. Med.* **2015**, *5*, a023267.
4. Nestle, F.O.; Di Meglio, P.; Qin, J.Z.; Nickoloff, B.J. Skin immune sentinels in health and disease. *Nat. Rev. Immunol.* **2009**, *9*, 679–691.
5. Negut, I.; Grumezescu, V.; Grumezescu, A.M. Treatment Strategies for Infected Wounds. *Molecules* **2018**, *23*, 2392.
6. Gurtner, G.C.; Werner, S.; Barrandon, Y.; Longaker, M.T. Wound repair and regeneration. *Nature* **2008**, *453*, 314–321.
7. Calvanese, L.; Brun, P.; Messina, G.M.L.; Russo, T.; Zamuner, A.; Falcigno, L.; D'Auria, G.; Gloria, A.; Vitagliano, L.; Marletta, G.; et al. EAK Hydrogels Cross-Linked by Disulfide Bonds: Cys Number and Position Are Matched to Performances. *ACS Biomater. Sci. Eng.* **2020**, *6*, 1154–1164.

8. Manso Silván, M.; Messina, G.M.L.; Montero, I.; Satriano, C.; Ruiz, J.P.G.; Marletta, G. Aminofunctionalization and sub-micrometer patterning on silicon through silane doped agarose hydrogels. *J. Mater. Chem.* **2009**, *19*, 5226–5233.
9. Farahani, M.; Shafiee, A. Wound Healing: From Passive to Smart Dressings. *Adv. Healthc. Mater.* **2021**, *10*, e2100477.
10. Memic, A.; Abudula, T.; Mohammed, H.S.; Joshi Navare, K.; Colombani, T.; Bencherif, S.A. Latest Progress in Electrospun Nanofibers for Wound Healing Applications. *ACS Appl. Bio Mater.* **2019**, *2*, 952–969.
11. Haik, J.; Kornhaber, R.; Blal, B.; Harats, M. The Feasibility of a Handheld Electrospinning Device for the Application of Nanofibrous Wound Dressings. *Adv. Wound Care (New Rochelle)* **2017**, *6*, 166–174.
12. Abrigo, M.; McArthur, S.L.; Kingshott, P. Electrospun nanofibers as dressings for chronic wound care: Advances, challenges, and future prospects. *Macromol. Biosci.* **2014**, *14*, 772–792.
13. Graca, M.F.P.; de Melo-Diogo, D.; Correia, I.J.; Moreira, A.F. Electrospun Asymmetric Membranes as Promising Wound Dressings: A Review. *Pharmaceutics* **2021**, *13*, 183.
14. Mousavi, S.M.; Zarei, M.; Hashemi, S.A.; Ramakrishna, S.; Chiang, W.-H.; Lai, C.W.; Gholami, A.; Omidifar, N.; Shokripour, M. Asymmetric Membranes: A Potential Scaffold for Wound Healing Applications. *Symmetry* **2020**, *12*, 1100.
15. Zhang, T.; Xu, H.; Zhang, Y.; Zhang, S.; Yang, X.; Wei, Y.; Huang, D.; Lian, X. Fabrication and characterization of double-layer asymmetric dressing through electrostatic spinning and 3D printing for skin wound repair. *Mater. Des.* **2022**, *218*, 110711.
16. Yu, B.; He, C.; Wang, W.; Ren, Y.; Yang, J.; Guo, S.; Zheng, Y.; Shi, X. Asymmetric Wettable Composite Wound Dressing Prepared by Electrospinning with Bioinspired Micropatterning Enhances Diabetic Wound Healing. *ACS Appl. Bio Mater.* **2020**, *3*, 5383–5394.
17. Xing, J.; Zhang, M.; Liu, X.; Wang, C.; Xu, N.; Xing, D. Multi-material electrospinning: From methods to biomedical applications. *Mater. Today Bio* **2023**, *21*, 100710.
18. Graca, M.F.P.; Miguel, S.P.; Cabral, C.S.D.; Correia, I.J. Hyaluronic acid-Based wound dressings: A review. *Carbohydr. Polym.* **2020**, *241*, 116364.
19. Frenkel, J.S. The role of hyaluronan in wound healing. *Int. Wound J.* **2014**, *11*, 159–163.
20. Chen, W.Y.J. Functions of Hyaluronan in Wound Repair. In *Hyaluronan*; Kennedy, J.F., Phillips, G.O., Williams, P.A., Eds.; Woodhead Publishing: Cambridge, UK, 2002; pp. 147–156.
21. Voigt, J.; Driver, V.R. Hyaluronic acid derivatives and their healing effect on burns, epithelial surgical wounds, and chronic wounds: A systematic review and meta-analysis of randomized controlled trials. *Wound Repair. Regen.* **2012**, *20*, 317–331.
22. Hintze, V.; Schnabelrauch, M.; Rother, S. Chemical Modification of Hyaluronan and Their Biomedical Applications. *Front. Chem.* **2022**, *10*, 830671.
23. Pepe, A.; Laezza, A.; Armiento, F.; Bochicchio, B. Chemical Modifications in Hyaluronic Acid-Based Electrospun Scaffolds. *Chempluschem* **2024**, *89*, e202300599.
24. Chanda, A.; Adhikari, J.; Ghosh, A.; Chowdhury, S.R.; Thomas, S.; Datta, P.; Saha, P. Electrospun chitosan/polycaprolactone-hyaluronic acid bilayered scaffold for potential wound healing applications. *Int. J. Biol. Macromol.* **2018**, *116*, 774–785.
25. Ebrahimi-Hosseinzadeh, B.; Pedram, M.; Hatamian-Zarmi, A.; Salahshour-Kordestani, S.; Rasti, M.; Mokhtari-Hosseini, Z.B.; Mir-Derikvand, M. In vivo evaluation of gelatin/hyaluronic acid nanofiber as Burn-wound healing and its comparison with ChitoHeal gel. *Fibers Polym.* **2016**, *17*, 820–826.
26. Ielo, I.; Bauso, L.V.; Laezza, A.; Campione, P.; Fabiano, L.; Pastorello, M.; Marino, A.; Laurita, A.; Pepe, A.; Bochicchio, B.; et al. In Vitro Assessment of Electrospun PVP+AgNPs Scaffolds for Bioactive Medical Use. *Int. J. Mol. Sci.* **2025**, *26*, 9114.
27. Kurakula, M.; Koteswara Rao, G.S.N. Moving polyvinyl pyrrolidone electrospun nanofibers and bioprinted scaffolds toward multidisciplinary biomedical applications. *Eur. Polym. J.* **2020**, *136*, 109919.
28. Schanté, C.E.; Zuber, G.; Herlin, C.; Vandamme, T.F. Improvement of hyaluronic acid enzymatic stability by the grafting of amino-acids. *Carbohydr. Polym.* **2012**, *87*, 2211–2216.
29. Schanté, C.E.; Zuber, G.; Herlin, C.; Vandamme, T.F. Chemical modifications of hyaluronic acid for the synthesis of derivatives for a broad range of biomedical applications. *Carbohydr. Polym.* **2011**, *85*, 469–489.
30. Adhikari, J.; Dasgupta, S.; Das, P.; Gouripriya, D.A.; Barui, A.; Basak, P.; Ghosh, M.; Saha, P. Bilayer regenerated cellulose/quaternized chitosan-hyaluronic acid/collagen electrospun scaffold for potential wound healing applications. *Int. J. Biol. Macromol.* **2024**, *261*, 129661.
31. Petrova, V.A.; Chernyakov, D.D.; Poshina, D.N.; Gofman, I.V.; Romanov, D.P.; Mishanin, A.I.; Golovkin, A.S.; Skorik, Y.A. Electrospun Bilayer Chitosan/Hyaluronan Material and Its Compatibility with Mesenchymal Stem Cells. *Materials* **2019**, *12*, 2016.

32. Arnal-Pastor, M.; Martínez Ramos, C.; Pérez Garnés, M.; Monleón Pradas, M.; Vallés Lluch, A. Electrospun adherent–antiadherent bilayered membranes based on cross-linked hyaluronic acid for advanced tissue engineering applications. *Mater. Sci. Eng. C* **2013**, *33*, 4086–4093.
33. Mohan, T.; Gürer, F.; Bračič, D.; Lackner, F.; Nagaraj, C.; Maver, U.; Gradišnik, L.; Finšgar, M.; Kargl, R.; Kleinschek, K.S. Functionalization of Polycaprolactone 3D Scaffolds with Hyaluronic Acid Glycine-Peptide Conjugates and Endothelial Cell Adhesion. *Biomacromolecules* **2025**, *26*, 1771–1787.
34. Laezza, A.; Pepe, A.; Solimando, N.; Armiento, F.; Oszust, F.; Duca, L.; Bochicchio, B. A Study on Thiol-Michael Addition to Semi-Synthetic Elastin-Hyaluronan Material for Electrospun Scaffolds. *Chempluschem* **2024**, *89*, e202300662.
35. Laezza, A.; Pepe, A.; Bochicchio, B. Elastin-Hyaluronan Bioconjugate as Bioactive Component in Electrospun Scaffolds. *Chem. A Eur. J.* **2022**, *28*, e202201959.
36. Tan, X.; Jain, E.; Barcellona, M.N.; Morris, E.; Neal, S.; Gupta, M.C.; Buchowski, J.M.; Kelly, M.; Setton, L.A.; Huebsch, N. Integrin and syndecan binding peptide-conjugated alginate hydrogel for modulation of nucleus pulposus cell phenotype. *Biomaterials* **2021**, *277*, 121113.
37. Sader, J.E.; Chon, J.W.M.; Mulvaney, P. Calibration of rectangular atomic force microscope cantilevers. *Rev. Sci. Instrum.* **1999**, *70*, 3967–3969.
38. Derjaguin, B.V.; Muller, V.M.; Toporov, Y.P. Effect of contact deformations on the adhesion of particles. *J. Colloid Interface Sci.* **1975**, *53*, 314–326.
39. Tüfekci, M.; Durak, S.G.; Pir, İ.; Acar, T.O.; Demirkol, G.T.; Tüfekci, N. Manufacturing, Characterisation and Mechanical Analysis of Polyacrylonitrile Membranes. *Polymers* **2020**, *12*, 2378.
40. Bruno, T.J.L.; David, R.L., Jr. (Eds.) *CRC Handbook of Chemistry and Physics*, 95th ed.; CRC Press: Boca Raton, FL, USA, 2014.
41. D'Amora, U.; Ronca, A.; Scialla, S.; Soriente, A.; Manini, P.; Phua, J.W.; Ottenheim, C.; Pezzella, A.; Calabrese, G.; Raucci, M.G.; et al. Bioactive Composite Methacrylated Gellan Gum for 3D-Printed Bone Tissue-Engineered Scaffolds. *Nanomaterials* **2023**, *13*, 772.
42. Szychlinska, M.A.; Calabrese, G.; Ravalli, S.; Parrinello, N.L.; Forte, S.; Castrogiovanni, P.; Pricoco, E.; Imbesi, R.; Castorina, S.; Leonardi, R.; et al. Cycloastragenol as an Exogenous Enhancer of Chondrogenic Differentiation of Human Adipose-Derived Mesenchymal Stem Cells. A Morphological Study. *Cells* **2020**, *9*, 347.
43. Nestor, G.; Sandström, C. NMR study of hydroxy and amide protons in hyaluronan polymers. *Carbohydr. Polym.* **2017**, *157*, 920–928.
44. Blundell, C.D.; DeAngelis, P.L.; Almond, A. Hyaluronan: The absence of amide-carboxylate hydrogen bonds and the chain conformation in aqueous solution are incompatible with stable secondary and tertiary structure models. *Biochem. J.* **2006**, *396*, 487–498.
45. Dodd, R.J.; Blundell, C.D.; Sattelle, B.M.; Enghild, J.J.; Milner, C.M.; Day, A.J. Chemical modification of hyaluronan oligosaccharides differentially modulates hyaluronan-hyaladherin interactions. *J. Biol. Chem.* **2024**, *300*, 107668.
46. Otto, K.E.; Hesse, S.; Wassermann, T.N.; Rice, C.A.; Suhm, M.A.; Stafforst, T.; Diederichsen, U. Temperature-dependent intensity anomalies in amino acid esters: Weak hydrogen bonds in protected glycine, alanine and valine. *Phys. Chem. Chem. Phys.* **2011**, *13*, 14119–14130.
47. Morgado, P.I.; Aguiar-Ricardo, A.; Correia, I.J. Asymmetric membranes as ideal wound dressings: An overview on production methods, structure, properties and performance relationship. *J. Membr. Sci.* **2015**, *490*, 139–151.
48. Grimaudo, M.A.; Concheiro, A.; Alvarez-Lorenzo, C. Crosslinked Hyaluronan Electrospun Nanofibers for Ferulic Acid Ocular Delivery. *Pharmaceutics* **2020**, *12*, 274.
49. Rnjak-Kovacina, J.; Weiss, A.S. Increasing the pore size of electrospun scaffolds. *Tissue Eng. Part. Rev.* **2011**, *17*, 365–372.
50. Schwartz, J.B. Log-Normal Distribution of Tablet Pore Diameters. *J. Pharm. Sci.* **1974**, *63*, 774–776.
51. Ambekar, R.S.; Kandasubramanian, B. Advancements in nanofibers for wound dressing: A review. *Eur. Polym. J.* **2019**, *117*, 304–336.
52. Saghazadeh, S.; Rinoldi, C.; Schot, M.; Kashaf, S.S.; Sharifi, F.; Jalilian, E.; Nuutila, K.; Giatsidis, G.; Mostafalu, P.; Derakhshandeh, H.; et al. Drug delivery systems and materials for wound healing applications. *Adv. Drug Deliv. Rev.* **2018**, *127*, 138–166.
53. Kitsara, M.; Blanquer, A.; Murillo, G.; Humblot, V.; De Braganca Vieira, S.; Nogues, C.; Ibanez, E.; Esteve, J.; Barrios, L. Permanently hydrophilic, piezoelectric PVDF nanofibrous scaffolds promoting unaided electromechanical stimulation on osteoblasts. *Nanoscale* **2019**, *11*, 8906–8917.

54. Piccirillo, G.; Feuerer, N.; Carvajal Berrio, D.A.; Layland, S.L.; Reimer Hinderer, S.; Bochicchio, B.; Schenke-Layland, K. Hyaluronic Acid-Functionalized Hybrid Gelatin–Poly-L-Lactide Scaffolds with Tunable Hydrophilicity. *Tissue Eng. Part. C Methods* **2021**, *27*, 589–604.
55. Di Mola, A.; Landi, M.R.; Massa, A.; D'Amora, U.; Guarino, V. Hyaluronic Acid in Biomedical Fields: New Trends from Chemistry to Biomaterial Applications. *Int. J. Mol. Sci.* **2022**, *23*, 14372.
56. Lewandowska, K.; Szulc, M. Characterisation of Hyaluronic Acid Blends Modified by Poly(N-Vinylpyrrolidone). *Molecules* **2021**, *26*, 5233.
57. Burdick, J.A.; Prestwich, G.D. Hyaluronic Acid Hydrogels for Biomedical Applications. *Adv. Mater.* **2011**, *23*, H41–H56.
58. Drobota, M.; Ursache, S.; Aflori, M. Surface Functionalities of Polymers for Biomaterial Applications. *Polymers* **2022**, *14*, 2307.
59. Kim, M.; Cha, C. Modulation of functional pendant chains within poly(ethylene glycol) hydrogels for refined control of protein release. *Sci. Rep.* **2018**, *8*, 4315.
60. Liang, Y.; Li, L.; Scott, R.A.; Kiick, K.L. 50th Anniversary Perspective: Polymeric Biomaterials: Diverse Functions Enabled by Advances in Macromolecular Chemistry. *Macromolecules* **2017**, *50*, 483–502.
61. Ní Annaidh, A.; Bruyère, K.; Destrade, M.; Gilchrist, M.D.; Otténio, M. Characterization of the anisotropic mechanical properties of excised human skin. *J. Mech. Behav. Biomed. Mater.* **2012**, *5*, 139–148.
62. Flynn, C.; Taberner, A.; Nielsen, P. Mechanical characterisation of in vivo human skin using a 3D force-sensitive micro-robot and finite element analysis. *Biomech. Model. Mechanobiol.* **2011**, *10*, 27–38.
63. Joodaki, H.; Panzer, M.B. Skin mechanical properties and modeling: A review. *Proc. Inst. Mech. Eng. H* **2018**, *232*, 323–343.
64. Chen, H.; Xue, H.; Zeng, H.; Dai, M.; Tang, C.; Liu, L. 3D printed scaffolds based on hyaluronic acid bioinks for tissue engineering: A review. *Biomater. Res.* **2023**, *27*, 137.
65. Humaira; Raza Bukhari, S.A.; Shakir, H.A.; Khan, M.; Saeed, S.; Ahmad, I.; Muzammil, K.; Franco, M.; Irfan, M.; Li, K. Hyaluronic acid-based nanofibers: Electrospun synthesis and their medical applications; recent developments and future perspective. *Front. Chem.* **2022**, *10*, 1092123.
66. Petrova, V.A.; Golovkin, A.S.; Mishanin, A.I.; Romanov, D.P.; Chernyakov, D.D.; Poshina, D.N.; Skorik, Y.A. Cytocompatibility of Bilayer Scaffolds Electrospun from Chitosan/Alginate-Chitin Nanowhiskers. *Biomedicines* **2020**, *8*, 305.
67. Niu, Y.; Galluzzi, M. Hyaluronic Acid/Collagen Nanofiber Tubular Scaffolds Support Endothelial Cell Proliferation, Phenotypic Shape and Endothelialization. *Nanomaterials* **2021**, *11*, 2334.
68. Mohammadalizadeh, Z.; Bahremandi-Toloue, E.; Karbasi, S. Synthetic-based blended electrospun scaffolds in tissue engineering applications. *J. Mater. Sci.* **2022**, *57*, 4020–4079.
69. Niemczyk-Soczynska, B.; Gradys, A.; Sajkiewicz, P. Hydrophilic Surface Functionalization of Electrospun Nanofibrous Scaffolds in Tissue Engineering. *Polymers* **2020**, *12*, 2636.
70. Ruccolo, L.; Evangelista, A.; Benazzo, M.; Conti, B.; Pisani, S. Electrospun Bio-Scaffolds for Mesenchymal Stem Cell-Mediated Neural Differentiation: Systematic Review of Advances and Future Directions. *Int. J. Mol. Sci.* **2025**, *26*, 9528.
71. El-Ghoul, Y.; Altuwayjiri, A.S.; Alharbi, G.A. Synthesis and characterization of new electrospun medical scaffold-based modified cellulose nanofiber and bioactive natural propolis for potential wound dressing applications. *Rsc Adv.* **2024**, *14*, 26183–26197.
72. Lopérgolo, L.C.; Lugão, A.B.; Catalani, L.H. Direct UV photocrosslinking of poly(N-vinyl-2-pyrrolidone) (PVP) to produce hydrogels. *Polymer* **2003**, *44*, 6217–6222.
73. Sionkowska, A.; Wisniewski, M.; Skopinska, J.; Vicini, S.; Marsano, E. The influence of UV irradiation on the mechanical properties of chitosan/poly(vinyl pyrrolidone) blends. *Polym. Degr. Stab.* **2005**, *88*, 261–267.